BLOW-UP OF COMPLEX SOLUTIONS OF THE 3-d NAVIER-STOKES EQUATIONS AND BEHAVIOR OF RELATED REAL SOLUTIONS

BLOW-UP OF COMPLEX SOLUTIONS OF THE 3-d NAVIER-STOKES EQUATIONS AND BEHAVIOR OF RELATED REAL SOLUTIONS

C. Boldrighini
Istituto Nazionale d'Alta Matematica
GNFM, unità locale Roma III

S. Frigio, and P. Maponi
Università di Camerino

1. INTRODUCTION

We consider the three-dimensional incompressible Navier-Stokes (NS) equations, in absence of boundary conditions and external forces:

1. INTRODUCTION

We consider the three-dimensional incompressible Navier-Stokes (NS) equations, in absence of boundary conditions and external forces:

$$\frac{\partial \mathbf{u}}{\partial t} + \sum_{j=1}^{3} u_j \frac{\partial}{\partial x_j}\mathbf{u} = \Delta \mathbf{u} - \nabla p, \qquad \mathbf{x} = (x_1, x_2, x_3) \in \mathbb{R}^3.$$

$$\nabla \cdot \mathbf{u} = 0, \qquad \mathbf{u}(\cdot, 0) = \mathbf{u}_0.$$

$\mathbf{u} : \mathbb{R}^3 \times [0, \infty) \to \mathbb{R}^3$ is the velocity field, p is the pressure and we assume for the viscosity $\nu = 1$ (always possible by rescaling).

1. INTRODUCTION

We consider the three-dimensional incompressible Navier-Stokes (NS) equations, in absence of boundary conditions and external forces:

$$\frac{\partial \mathbf{u}}{\partial t} + \sum_{j=1}^{3} u_j \frac{\partial}{\partial x_j}\mathbf{u} = \Delta \mathbf{u} - \nabla p, \qquad \mathbf{x} = (x_1, x_2, x_3) \in \mathbb{R}^3.$$

$$\nabla \cdot \mathbf{u} = 0, \qquad \mathbf{u}(\cdot, 0) = \mathbf{u}_0.$$

$\mathbf{u} : \mathbb{R}^3 \times [0, \infty) \to \mathbb{R}^3$ is the velocity field, p is the pressure and we assume for the viscosity $\nu = 1$ (always possible by rescaling).

In spite of considerable progress, it is still unknown whether there are initial conditions for which the solution becomes singular in a finite time (global regularity problem).

1. Introduction

The singular solutions, if they exist, would have physical relevance:

1. Introduction

The singular solutions, if they exist, would have physical relevance: describe phenomena such as hurricanes,

1. Introduction

The singular solutions, if they exist, would have physical relevance: describe phenomena such as hurricanes, i.e., a sudden concentration of energy in a small space region.

1. Introduction

The singular solutions, if they exist, would have physical relevance: describe phenomena such as hurricanes, i.e., a sudden concentration of energy in a small space region. There is no effective model describing such phenomena.

1. Introduction

The singular solutions, if they exist, would have physical relevance: describe phenomena such as hurricanes, i.e., a sudden concentration of energy in a small space region. There is no effective model describing such phenomena.

For a recent contribution on the global regularity problem with extensive literature:

1. Introduction

The singular solutions, if they exist, would have physical relevance: describe phenomena such as hurricanes, i.e., a sudden concentration of energy in a small space region. There is no effective model describing such phenomena.

For a recent contribution on the global regularity problem with extensive literature:

T. Tao: "Finite-time blowup for an averaged three-dimensional Navier-Stokes Equation". arXiv:1402.0290v2 [math.AP] 6 Feb 2014,

1. Introduction

The singular solutions, if they exist, would have physical relevance: describe phenomena such as hurricanes, i.e., a sudden concentration of energy in a small space region. There is no effective model describing such phenomena.

For a recent contribution on the global regularity problem with extensive literature:

T. Tao: "Finite-time blowup for an averaged three-dimensional Navier-Stokes Equation". arXiv:1402.0290v2 [math.AP] 6 Feb 2014,

where a blowup is proved for a modified NS equations, which preserve the the *energy identity*

$$E(t) + \int_0^t S(\tau) d\tau = E(0),$$

$E(t)$ is the total energy and $S(t)$ the total enstrophy

$$E(t) = \frac{1}{2} \int_{\mathbb{R}^3} |\mathbf{u}(\mathbf{x}, t)|^2 d\mathbf{x}, \qquad S(t) = \int_{\mathbb{R}^3} |\nabla \mathbf{u}(\mathbf{x}, t)|^2 d\mathbf{x}.$$

1. Introduction

In 2008 Li and Sinai proved that the NS equation in the whole space and with no external forces with do indeed blow up after a finite time for some class of smooth complex initial data.

In 2008 Li and Sinai proved that the NS equation in the whole space and with no external forces with do indeed blow up after a finite time for some class of smooth complex initial data.

Li, D. and Sinai, Ya. G. 2008. *Blowups of complex solutions of the 3D Navier-Stokes system and renormalization group method.* J. Eur. Math. Soc. **10**, 267–313

In 2008 Li and Sinai proved that the NS equation in the whole space and with no external forces with do indeed blow up after a finite time for some class of smooth complex initial data.

Li, D. and Sinai, Ya. G. 2008. *Blowups of complex solutions of the 3D Navier-Stokes system and renormalization group method.* J. Eur. Math. Soc. **10**, 267–313

Complex solutions with blow-up have been established also for the Burgers equations and other models:

In 2008 Li and Sinai proved that the NS equation in the whole space and with no external forces with do indeed blow up after a finite time for some class of smooth complex initial data.

Li, D. and Sinai, Ya. G. 2008. *Blowups of complex solutions of the 3D Navier-Stokes system and renormalization group method.* J. Eur. Math. Soc. **10**, 267–313

Complex solutions with blow-up have been established also for the Burgers equations and other models:

Li, D. and Sinai, Ya. G. 2010. *Singularities of complex-valued solutions of the two-dimensional Burgers system.* J. Math. Phys. **51**, 01525

Pauls, W. 2011. *Some remarks on Li-Sinai-type solutions of the Burgers equation.* J. Phys. A: Math. Theor. **44** 285209

In general, simulating solutions of the 3-d NS equations is a very challenging task even for the last generation of supercomputers.

In general, simulating solutions of the 3-d NS equations is a very challenging task even for the last generation of supercomputers.

We will also report results from computer simulations on the behavior of a class of related real solutions of the NS equations.

In general, simulating solutions of the 3-d NS equations is a very challenging task even for the last generation of supercomputers.

We will also report results from computer simulations on the behavior of a class of related real solutions of the NS equations.

The starting point is a reformulation of the 3-d NS equations into a convolution integral equation,

In general, simulating solutions of the 3-d NS equations is a very challenging task even for the last generation of supercomputers.

We will also report results from computer simulations on the behavior of a class of related real solutions of the NS equations.

The starting point is a reformulation of the 3-d NS equations into a convolution integral equation, by means of the modified Fourier transform

$$\mathbf{v}(\mathbf{k}, t) = \frac{i}{(2\pi)^3} \int_{\mathbb{R}^3} \mathbf{u}(\mathbf{x}, t) e^{i(\mathbf{k}, x)} d\mathbf{x}.$$

The NS equations go, by a Duhamel formula, into

$$\mathbf{v}(\mathbf{k},t) = e^{-t\mathbf{k}^2}\mathbf{v}_0(\mathbf{k}) +$$

$$+ \int_0^t e^{-(t-s)\mathbf{k}^2} ds \int_{\mathbb{R}^3} \langle \mathbf{v}(\mathbf{k}-\mathbf{k}',s), \mathbf{k}\rangle \; P_{\mathbf{k}} \; \mathbf{v}(\mathbf{k}',s) \; d\mathbf{k}',$$

The NS equations go, by a Duhamel formula, into

$$\mathbf{v}(\mathbf{k},t) = e^{-t\mathbf{k}^2}\mathbf{v}_0(\mathbf{k}) +$$

$$+ \int_0^t e^{-(t-s)\mathbf{k}^2} ds \int_{\mathbb{R}^3} \langle \mathbf{v}(\mathbf{k}-\mathbf{k}',s),\mathbf{k}\rangle \; P_{\mathbf{k}} \; \mathbf{v}(\mathbf{k}',s) \; d\mathbf{k}',$$

where $\mathbf{v}_0(\mathbf{k}) = \mathbf{v}(\mathbf{k},0)$ is the initial data and $P_{\mathbf{k}}$ the orthogonal projector expressing incompressibility:

$$P_{\mathbf{k}}\mathbf{v} = \mathbf{v} - \frac{\langle \mathbf{v},\mathbf{k}\rangle}{\mathbf{k}^2}\mathbf{k}.$$

The NS equations go, by a Duhamel formula, into

$$\mathbf{v}(\mathbf{k},t) = e^{-t\mathbf{k}^2}\mathbf{v}_0(\mathbf{k}) +$$

$$+ \int_0^t e^{-(t-s)\mathbf{k}^2} ds \int_{\mathbb{R}^3} \langle \mathbf{v}(\mathbf{k}-\mathbf{k}',s), \mathbf{k}\rangle \; P_{\mathbf{k}} \; \mathbf{v}(\mathbf{k}',s) \; d\mathbf{k}',$$

where $\mathbf{v}_0(\mathbf{k}) = \mathbf{v}(\mathbf{k},0)$ is the initial data and $P_{\mathbf{k}}$ the orthogonal projector expressing incompressibility:

$$P_{\mathbf{k}}\mathbf{v} = \mathbf{v} - \frac{\langle \mathbf{v}, \mathbf{k}\rangle}{\mathbf{k}^2}\mathbf{k}.$$

The integral equation is considered for real functions $\mathbf{v}(\mathbf{k},t)$.

The NS equations go, by a Duhamel formula, into

$$\mathbf{v}(\mathbf{k},t) = e^{-t\mathbf{k}^2}\mathbf{v}_0(\mathbf{k}) +$$

$$+ \int_0^t e^{-(t-s)\mathbf{k}^2} ds \int_{\mathbb{R}^3} \langle \mathbf{v}(\mathbf{k}-\mathbf{k}',s), \mathbf{k}\rangle \; P_{\mathbf{k}} \; \mathbf{v}(\mathbf{k}',s) \; d\mathbf{k}',$$

where $\mathbf{v}_0(\mathbf{k}) = \mathbf{v}(\mathbf{k},0)$ is the initial data and $P_{\mathbf{k}}$ the orthogonal projector expressing incompressibility:

$$P_{\mathbf{k}}\mathbf{v} = \mathbf{v} - \frac{\langle \mathbf{v}, \mathbf{k}\rangle}{\mathbf{k}^2}\mathbf{k}.$$

The integral equation is considered for real functions $\mathbf{v}(\mathbf{k},t)$. The antitrasform $\mathbf{u}(\mathbf{x},t)$ is complex in general.

The NS equations go, by a Duhamel formula, into

$$\mathbf{v}(\mathbf{k},t) = e^{-t\mathbf{k}^2}\mathbf{v}_0(\mathbf{k}) +$$

$$+ \int_0^t e^{-(t-s)\mathbf{k}^2} ds \int_{\mathbb{R}^3} \langle \mathbf{v}(\mathbf{k}-\mathbf{k}',s), \mathbf{k}\rangle \; P_{\mathbf{k}} \; \mathbf{v}(\mathbf{k}',s) \; d\mathbf{k}',$$

where $\mathbf{v}_0(\mathbf{k}) = \mathbf{v}(\mathbf{k},0)$ is the initial data and $P_{\mathbf{k}}$ the orthogonal projector expressing incompressibility:

$$P_{\mathbf{k}}\mathbf{v} = \mathbf{v} - \frac{\langle \mathbf{v}, \mathbf{k}\rangle}{\mathbf{k}^2}\mathbf{k}.$$

The integral equation is considered for real functions $\mathbf{v}(\mathbf{k},t)$. The antitrasform $\mathbf{u}(\mathbf{x},t)$ is complex in general.

If however $\mathbf{v}(\mathbf{k},t)$ is odd in $\mathbf{k}$ then $\mathbf{u}(\mathbf{x},t)$ is real and odd in $\mathbf{x}$.

Behavior of energy and enstrophy at $t \uparrow \tau$.

Behavior of energy and enstrophy at $t \uparrow \tau$.

The total energy $E(t)$ and the total enstrophy $S(t)$ blow up as $t \uparrow \tau$, with different rates for the two types $\alpha = I, II$:

Behavior of energy and enstrophy at $t \uparrow \tau$.

The total energy $E(t)$ and the total enstrophy $S(t)$ blow up as $t \uparrow \tau$, with different rates for the two types $\alpha = I, II$:

$$E(t) = \frac{(2\pi)^3}{2} \int_{\mathbb{R}^3} |\mathbf{v}(\mathbf{k}, t)|^2 d\mathbf{k}, \sim \frac{C_E^{(\alpha)}}{(\tau - t)^{\beta_\alpha}},$$

$$S(t) = (2\pi)^3 \int_{\mathbb{R}^3} \mathbf{k}^2 |\mathbf{v}(\mathbf{k}, t)|^2 d\mathbf{k} \sim \frac{C_S^{(\alpha)}}{(\tau - t)^{\beta_\alpha + 2}},$$

Behavior of energy and enstrophy at $t \uparrow \tau$.

The total energy $E(t)$ and the total enstrophy $S(t)$ blow up as $t \uparrow \tau$, with different rates for the two types $\alpha = I, II$:

$$E(t) = \frac{(2\pi)^3}{2} \int_{\mathbb{R}^3} |\mathbf{v}(\mathbf{k}, t)|^2 d\mathbf{k}, \sim \frac{C_E^{(\alpha)}}{(\tau - t)^{\beta_\alpha}},$$

$$S(t) = (2\pi)^3 \int_{\mathbb{R}^3} \mathbf{k}^2 |\mathbf{v}(\mathbf{k}, t)|^2 d\mathbf{k} \sim \frac{C_S^{(\alpha)}}{(\tau - t)^{\beta_\alpha + 2}},$$

where $\beta_I = 1$, $\beta_{II} = \frac{1}{2}$ and $C_E^{(\alpha)}, C_S^{(\alpha)}$ are constants.

The rigorous results give the following predictions:

The rigorous results give the following predictions:

i) The solution has its main support within a thin cone along the k_3-axis,

The rigorous results give the following predictions:

i) The solution has its main support within a thin cone along the k_3-axis, and is represented as a sum of modulated gaussian terms concentrated around the points $(0, 0, p\ a)$ and multiplied by $\exp\{-\kappa\ p(\tau - t)\}$;

The rigorous results give the following predictions:

i) The solution has its main support within a thin cone along the k_3-axis, and is represented as a sum of modulated gaussian terms concentrated around the points $(0, 0, p\ a)$ and multiplied by $\exp\{-\kappa\ p(\tau - t)\}$;

ii) For large k_3, the velocity field is approximately orthogonal to the k_3-axis and its direction is approximately radial;

The rigorous results give the following predictions:

i) The solution has its main support within a thin cone along the k_3-axis, and is represented as a sum of modulated gaussian terms concentrated around the points $(0, 0, p\ a)$ and multiplied by $\exp\{-\kappa\ p(\tau - t)\}$;

ii) For large k_3, the velocity field is approximately orthogonal to the k_3-axis and its direction is approximately radial;

iii) The solutions converge point-wise in $\mathbf{k}$-space as $t \uparrow \tau$,

The rigorous results give the following predictions:

i) The solution has its main support within a thin cone along the k_3-axis, and is represented as a sum of modulated gaussian terms concentrated around the points $(0, 0, p\ a)$ and multiplied by $\exp\{-\kappa\ p(\tau - t)\}$;

ii) For large k_3, the velocity field is approximately orthogonal to the k_3-axis and its direction is approximately radial;

iii) The solutions converge point-wise in $\mathbf{k}$-space as $t \uparrow \tau$, while $E(t)$ and $S(t)$ diverge as inverse powers of $\tau - t$.

3. LI-SINAI SOLUTIONS. SIMULATIONS.

The computer simulations for the complex Li-Sinai solutions reveal important properties which are not, so far, predicted by the theory.

3. LI-SINAI SOLUTIONS. SIMULATIONS.

The computer simulations for the complex Li-Sinai solutions reveal important properties which are not, so far, predicted by the theory.
Computer simulations for the Li-Sinai solutions were first performed by Arnol'd and Khokhlov in 2009.

3. LI-SINAI SOLUTIONS. SIMULATIONS.

The computer simulations for the complex Li-Sinai solutions reveal important properties which are not, so far, predicted by the theory.
Computer simulations for the Li-Sinai solutions were first performed by Arnol'd and Khokhlov in 2009. However, due to computational limitations, they could only get a qualitative description of the blow-up.

I report the results of simulations performed at CINECA (Bologna, Italy) on the Fermi Supercomputer.

I report the results of simulations performed at CINECA (Bologna, Italy) on the Fermi Supercomputer. They are obtained by implementation of a computational scheme for the NS equations in integral form,

I report the results of simulations performed at CINECA (Bologna, Italy) on the Fermi Supercomputer. They are obtained by implementation of a computational scheme for the NS equations in integral form, and can be used for a class of complex and real solutions of the NS and similar equation.

I report the results of simulations performed at CINECA (Bologna, Italy) on the Fermi Supercomputer. They are obtained by implementation of a computational scheme for the NS equations in integral form, and can be used for a class of complex and real solutions of the NS and similar equation.

The main difficulty for the simulations are:

I report the results of simulations performed at CINECA (Bologna, Italy) on the Fermi Supercomputer. They are obtained by implementation of a computational scheme for the NS equations in integral form, and can be used for a class of complex and real solutions of the NS and similar equation.

The main difficulty for the simulations are:
i) the blow-up takes place in a very short time $\approx 10^{-5}$ time units (t.u),

I report the results of simulations performed at CINECA (Bologna, Italy) on the Fermi Supercomputer. They are obtained by implementation of a computational scheme for the NS equations in integral form, and can be used for a class of complex and real solutions of the NS and similar equation.

The main difficulty for the simulations are:
i) the blow-up takes place in a very short time $\approx 10^{-5}$ time units (t.u), so that the time step has to be small;

I report the results of simulations performed at CINECA (Bologna, Italy) on the Fermi Supercomputer. They are obtained by implementation of a computational scheme for the NS equations in integral form, and can be used for a class of complex and real solutions of the NS and similar equation.

The main difficulty for the simulations are:
i) the blow-up takes place in a very short time $\approx 10^{-5}$ time units (t.u), so that the time step has to be small;
ii) the support of the solution goes away in the k_3 direction as $t \uparrow \tau$.

According to a preliminary screening on a sample of "'good' initial data it appears that the "best" initial data are

$$\mathbf{v}_0^{\pm}(\mathbf{k}) = \pm\, K\, \bar{\mathbf{v}}_0(\mathbf{k}),$$

According to a preliminary screening on a sample of "'good' initial data it appears that the "best" initial data are

$$\mathbf{v}_0^{\pm}(\mathbf{k}) = \pm\, K\, \bar{\mathbf{v}}_0(\mathbf{k}),$$

$$\bar{\mathbf{v}}_0(\mathbf{k}) = \left(k_1, k_2, -\frac{k_1^2 + k_2^2}{k_3}\right) g^{(3)}(\mathbf{k} - \mathbf{k}^{(0)}) \mathbb{I}_D(\mathbf{k} - \mathbf{k}^{(0)}),$$

According to a preliminary screening on a sample of "'good' initial data it appears that the "best" initial data are

$$\mathbf{v}_0^{\pm}(\mathbf{k}) = \pm\, K\, \bar{\mathbf{v}}_0(\mathbf{k}),$$

$$\bar{\mathbf{v}}_0(\mathbf{k}) = \left(k_1, k_2, -\frac{k_1^2 + k_2^2}{k_3}\right) g^{(3)}(\mathbf{k} - \mathbf{k}^{(0)}) \mathbb{I}_D(\mathbf{k} - \mathbf{k}^{(0)}),$$

where $\mathbf{k}^{(0)} = (0, 0, a)$,

According to a preliminary screening on a sample of "'good' initial data it appears that the "best" initial data are

$$\mathbf{v}_0^{\pm}(\mathbf{k}) = \pm\, K\, \bar{\mathbf{v}}_0(\mathbf{k}),$$

$$\bar{\mathbf{v}}_0(\mathbf{k}) = \left(k_1, k_2, -\frac{k_1^2 + k_2^2}{k_3}\right) g^{(3)}(\mathbf{k} - \mathbf{k}^{(0)}) \mathbb{I}_D(\mathbf{k} - \mathbf{k}^{(0)}),$$

where $\mathbf{k}^{(0)} = (0, 0, a)$, $g^{(3)}$ is the standard gaussian on $\mathbb{R}^3$,

According to a preliminary screening on a sample of "'good' initial data it appears that the "best" initial data are

$$\mathbf{v}_0^{\pm}(\mathbf{k}) = \pm\, K\, \bar{\mathbf{v}}_0(\mathbf{k}),$$

$$\bar{\mathbf{v}}_0(\mathbf{k}) = \left(k_1, k_2, -\frac{k_1^2 + k_2^2}{k_3}\right) g^{(3)}(\mathbf{k} - \mathbf{k}^{(0)}) \mathbb{I}_D(\mathbf{k} - \mathbf{k}^{(0)}),$$

where $\mathbf{k}^{(0)} = (0, 0, a)$, $g^{(3)}$ is the standard gaussian on $\mathbb{R}^3$, $\mathbb{I}_D$ is the indicator function of the set $D = \{\mathbf{k} : |\mathbf{k}| \leq 17\}$, and in all cases $a \geq 20$.

According to a preliminary screening on a sample of "'good' initial data it appears that the "best" initial data are

$$\mathbf{v}_0^{\pm}(\mathbf{k}) = \pm\, K\, \bar{\mathbf{v}}_0(\mathbf{k}),$$

$$\bar{\mathbf{v}}_0(\mathbf{k}) = \left(k_1, k_2, -\frac{k_1^2 + k_2^2}{k_3}\right) g^{(3)}(\mathbf{k} - \mathbf{k}^{(0)}) \mathbb{I}_D(\mathbf{k} - \mathbf{k}^{(0)}),$$

where $\mathbf{k}^{(0)} = (0, 0, a)$, $g^{(3)}$ is the standard gaussian on $\mathbb{R}^3$, $\mathbb{I}_D$ is the indicator function of the set $D = \{\mathbf{k} : |\mathbf{k}| \leq 17\}$, and in all cases $a \geq 20$.

The positive constant K controls the initial energy.

According to a preliminary screening on a sample of "'good' initial data it appears that the "best" initial data are

$$\mathbf{v}_0^{\pm}(\mathbf{k}) = \pm\, K\, \bar{\mathbf{v}}_0(\mathbf{k}),$$

$$\bar{\mathbf{v}}_0(\mathbf{k}) = \left(k_1, k_2, -\frac{k_1^2 + k_2^2}{k_3}\right) g^{(3)}(\mathbf{k} - \mathbf{k}^{(0)}) \mathbb{I}_D(\mathbf{k} - \mathbf{k}^{(0)}),$$

where $\mathbf{k}^{(0)} = (0, 0, a)$, $g^{(3)}$ is the standard gaussian on $\mathbb{R}^3$, $\mathbb{I}_D$ is the indicator function of the set $D = \{\mathbf{k} : |\mathbf{k}| \leq 17\}$, and in all cases $a \geq 20$.

The positive constant K controls the initial energy.

We get solutions of type I for the initial data $\mathbf{v}_0^+$,

According to a preliminary screening on a sample of "'good' initial data it appears that the "best" initial data are

$$\mathbf{v}_0^{\pm}(\mathbf{k}) = \pm\, K\, \bar{\mathbf{v}}_0(\mathbf{k}),$$

$$\bar{\mathbf{v}}_0(\mathbf{k}) = \left(k_1, k_2, -\frac{k_1^2 + k_2^2}{k_3}\right) g^{(3)}(\mathbf{k} - \mathbf{k}^{(0)}) \mathbb{I}_D(\mathbf{k} - \mathbf{k}^{(0)}),$$

where $\mathbf{k}^{(0)} = (0, 0, a)$, $g^{(3)}$ is the standard gaussian on $\mathbb{R}^3$, $\mathbb{I}_D$ is the indicator function of the set $D = \{\mathbf{k} : |\mathbf{k}| \leq 17\}$, and in all cases $a \geq 20$.

The positive constant K controls the initial energy.

We get solutions of type *I* for the initial data $\mathbf{v}_0^+$, and of type *II* (alternating signs) for $\mathbf{v}_0^-$.

If K is large enough,

If K is large enough, so that for the initial energy $E_0 > 25,000$, the solution blows up after a time of the order 10^{-3} t.u.

If K is large enough, so that for the initial energy $E_0 > 25,000$, the solution blows up after a time of the order 10^{-3} t.u. The solutions "stays quiet" for about 10^{-3} t.u., with energy and enstrophy decreasing,

If K is large enough, so that for the initial energy $E_0 > 25,000$, the solution blows up after a time of the order 10^{-3} t.u. The solutions "stays quiet" for about 10^{-3} t.u., with energy and enstrophy decreasing, then both quantities increase rapidly, leading to a blow-up in a time of the order 10^{-5}.

If K is large enough, so that for the initial energy $E_0 > 25,000$, the solution blows up after a time of the order 10^{-3} t.u. The solutions "stays quiet" for about 10^{-3} t.u., with energy and enstrophy decreasing, then both quantities increase rapidly, leading to a blow-up in a time of the order 10^{-5}.

Most simulations were done for solutions of type II.

If K is large enough, so that for the initial energy $E_0 > 25,000$, the solution blows up after a time of the order 10^{-3} t.u. The solutions "stays quiet" for about 10^{-3} t.u., with energy and enstrophy decreasing, then both quantities increase rapidly, leading to a blow-up in a time of the order 10^{-5}.

Most simulations were done for solutions of type II. Their behavior is more similar to that of the related real solutions.

If K is large enough, so that for the initial energy $E_0 > 25,000$, the solution blows up after a time of the order 10^{-3} t.u. The solutions "stays quiet" for about 10^{-3} t.u., with energy and enstrophy decreasing, then both quantities increase rapidly, leading to a blow-up in a time of the order 10^{-5}.

Most simulations were done for solutions of type II. Their behavior is more similar to that of the related real solutions.

The mesh R in $\mathbf{k}$-space is taken with step 1:

$$R = [-127, 127] \times [-127, 127] \times [-19, L] \subset \mathbb{Z}^3,$$

where the critical parameter L takes the values $2028, 2528, 3028$.

If K is large enough, so that for the initial energy $E_0 > 25,000$, the solution blows up after a time of the order 10^{-3} t.u. The solutions "stays quiet" for about 10^{-3} t.u., with energy and enstrophy decreasing, then both quantities increase rapidly, leading to a blow-up in a time of the order 10^{-5}.

Most simulations were done for solutions of type II. Their behavior is more similar to that of the related real solutions.

The mesh R in $\mathbf{k}$-space is taken with step 1:

$$R = [-127, 127] \times [-127, 127] \times [-19, L] \subset \mathbb{Z}^3,$$

where the critical parameter L takes the values $2028, 2528, 3028$. Control simulations with finer meshes confirm stability.

3. Li-Sinai solutions: simulations.

For the description of the behavior we use the energy and enstrophy marginals in $\mathbf{k}$ along the main axis

$$E_3(k_3, t) = \frac{1}{2} \int_{\mathbb{R}\times\mathbb{R}} dk_1 dk_2 |\mathbf{v}(\mathbf{k}, t)|^2,$$

$$S_3(k_3, t) = \int_{\mathbb{R}\times\mathbb{R}} dk_1 dk_2 |\mathbf{k}|^2 |\mathbf{v}(\mathbf{k}, t)|^2$$

3. Li-Sinai solutions: simulations.

For the description of the behavior we use the energy and enstrophy marginals in $\mathbf{k}$ along the main axis

$$E_3(k_3,t) = \frac{1}{2}\int_{\mathbb{R}\times\mathbb{R}} dk_1 dk_2 |\mathbf{v}(\mathbf{k},t)|^2,$$

$$S_3(k_3,t) = \int_{\mathbb{R}\times\mathbb{R}} dk_1 dk_2 |\mathbf{k}|^2 |\mathbf{v}(\mathbf{k},t)|^2$$

and the analogous marginals $E_j(k_j,t)$, $S_j(k_j,t)$, $j=1,2$.

3. Li-Sinai solutions: simulations.

For the description of the behavior we use the energy and enstrophy marginals in $\mathbf{k}$ along the main axis

$$E_3(k_3,t) = \frac{1}{2}\int_{\mathbb{R}\times\mathbb{R}} dk_1 dk_2 |\mathbf{v}(\mathbf{k},t)|^2,$$

$$S_3(k_3,t) = \int_{\mathbb{R}\times\mathbb{R}} dk_1 dk_2 |\mathbf{k}|^2 |\mathbf{v}(\mathbf{k},t)|^2$$

and the analogous marginals $E_j(k_j,t)$, $S_j(k_j,t)$, $j=1,2$.

The marginals in $\mathbf{x}$-space are denoted $\tilde{E}_j(x_j,t)$, $\tilde{S}_j(x_j,t)$, $j=1,2,3$, with

$$\tilde{E}_3(k_3,t) = \frac{1}{2}\int_{\mathbb{R}\times\mathbb{R}} dx_1 dx_2 |\mathbf{u}(\mathbf{x},t)|^2,$$

$$\tilde{S}_3(k_3,t) = \int_{\mathbb{R}\times\mathbb{R}} dx_1 dx_2 |\nabla\mathbf{u}(\mathbf{x},t)|^2,$$

etc.

We now illustrate some of the main features of the solutions near the blow-up provided by the computer simulations.

We now illustrate some of the main features of the solutions near the blow-up provided by the computer simulations.

- The component of $\mathbf{v}(\mathbf{k}, t)$ orthogonal to the k_3-axis is roughly radial already at the beginning of the blow-up and for relatively small k_3.

We now illustrate some of the main features of the solutions near the blow-up provided by the computer simulations.

- The component of $\mathbf{v}(\mathbf{k}, t)$ orthogonal to the k_3-axis is roughly radial already at the beginning of the blow-up and for relatively small k_3.

- For k_1 and k_2 fixed the type II solutions describe, as a function of k_3 a damped oscillation with approximate period $2a$ and vanish on the planes $k_3 \approx (j + \frac{1}{2})a$.

We now illustrate some of the main features of the solutions near the blow-up provided by the computer simulations.

- The component of $\mathbf{v}(\mathbf{k}, t)$ orthogonal to the k_3-axis is roughly radial already at the beginning of the blow-up and for relatively small k_3.

- For k_1 and k_2 fixed the type II solutions describe, as a function of k_3 a damped oscillation with approximate period $2a$ and vanish on the planes $k_3 \approx (j + \frac{1}{2})a$.

- The total enstrophy $S(t)$ starts growing much earlier than the total energy $E(t)$.

We now illustrate some of the main features of the solutions near the blow-up provided by the computer simulations.

- The component of $\mathbf{v}(\mathbf{k}, t)$ orthogonal to the k_3-axis is roughly radial already at the beginning of the blow-up and for relatively small k_3.

- For k_1 and k_2 fixed the type *II* solutions describe, as a function of k_3 a damped oscillation with approximate period $2a$ and vanish on the planes $k_3 \approx (j + \frac{1}{2})a$.

- The total enstrophy $S(t)$ starts growing much earlier than the total energy $E(t)$.

- The solution of type *I* blow up much earlier than the solutions of type *II* with the same initial energy and same a.

3. Li-Sinai solutions: simulations. The fixed point $\mathbf{H}^{(0)}$.

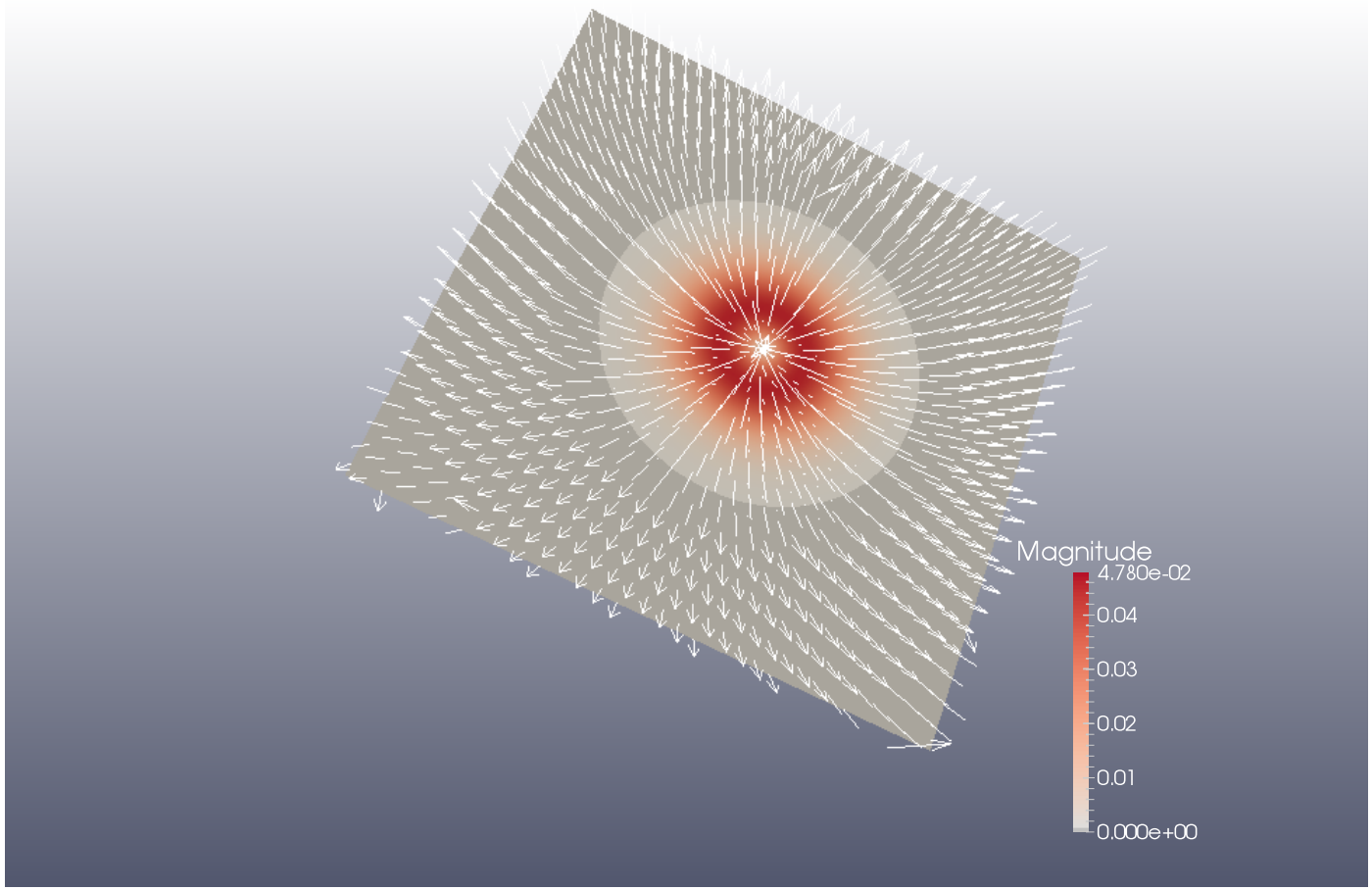

Figure 1: *Type II*, $a = 20$, $E_0 = 5 \times 10^4$. *The arrows indicate the direction of* $\mathbf{v}(\mathbf{k}, t)$ *on a regular point lattice on a section of the plane* $k_3 = 100$ *with sides of length* 100, $t = 1521 \times 10^{-7}$. *Simulation range* $k_3 \in [-19, 2528]$. *Magnitude refers to* $|\mathbf{v}(\mathbf{k}, t)|$. *In the grey external region* $|\mathbf{v}(\mathbf{k}, t)| < 10^{-6}$.

3. Li-Sinai solutions: simulations. Oscillations type I.

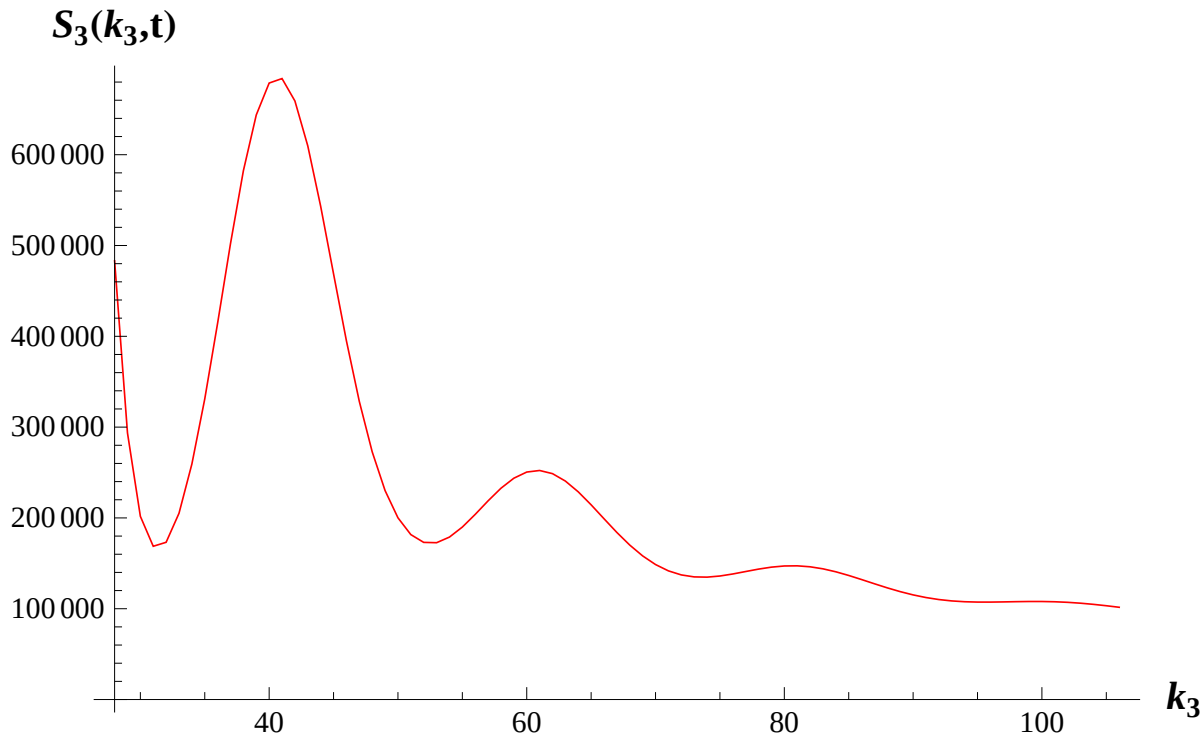

Figure 2: *Type I*, $a = 20$, $E_0 = 5 \times 10^4$. *Enstrophy marginal density* $S_3(k_3, t)$ *at the beginning of the blow-up.* $t = 900 \times 10^{-7}$. *Simulation range* $k_3 \in [-19, 2528]$.

3. Li-Sinai solutions: simulations. Oscillations type II.

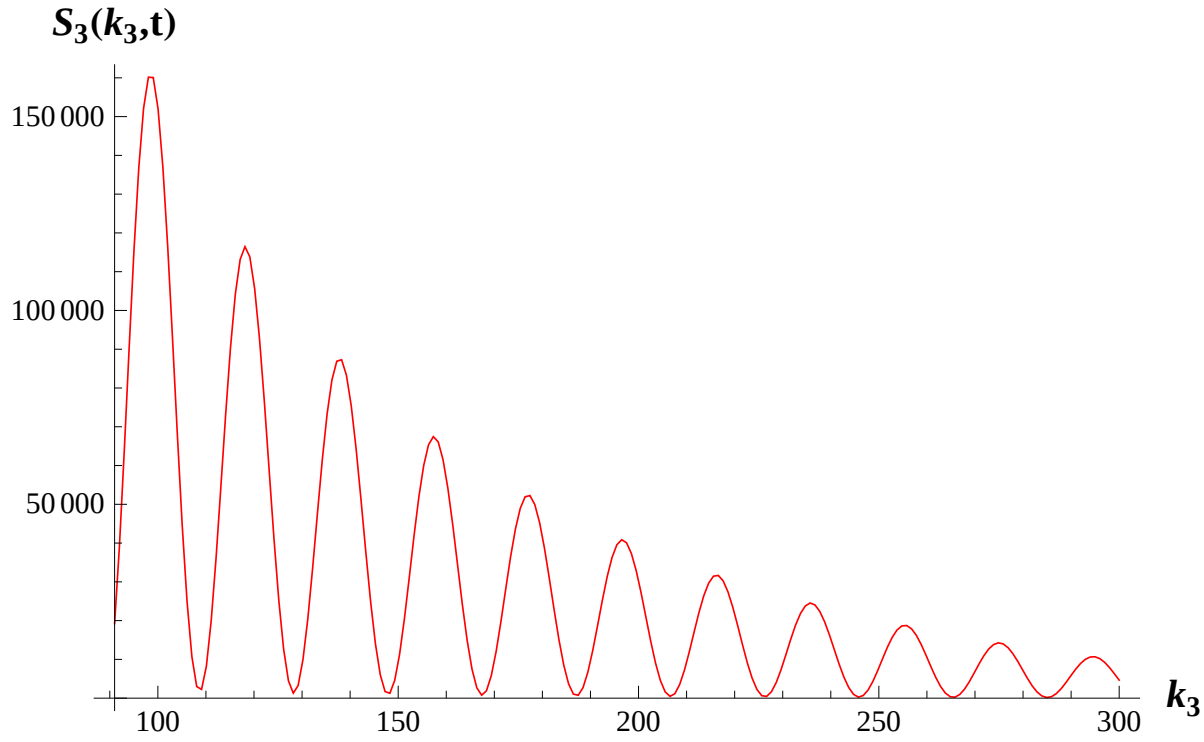

Figure 3: *Type II*, $a = 20$, $E_0 = 5 \times 10^4$. *Enstrophy marginal density* $S_3(k_3, t)$ *at the beginning of the blow-up.* $t = 1125 \times 10^{-7}$. *The zeroes are approximately periodic with period a. Simulation range* $k_3 \in [-19, 2528]$.

3. Li-Sinai solutions: simulations. Oscillations type II.

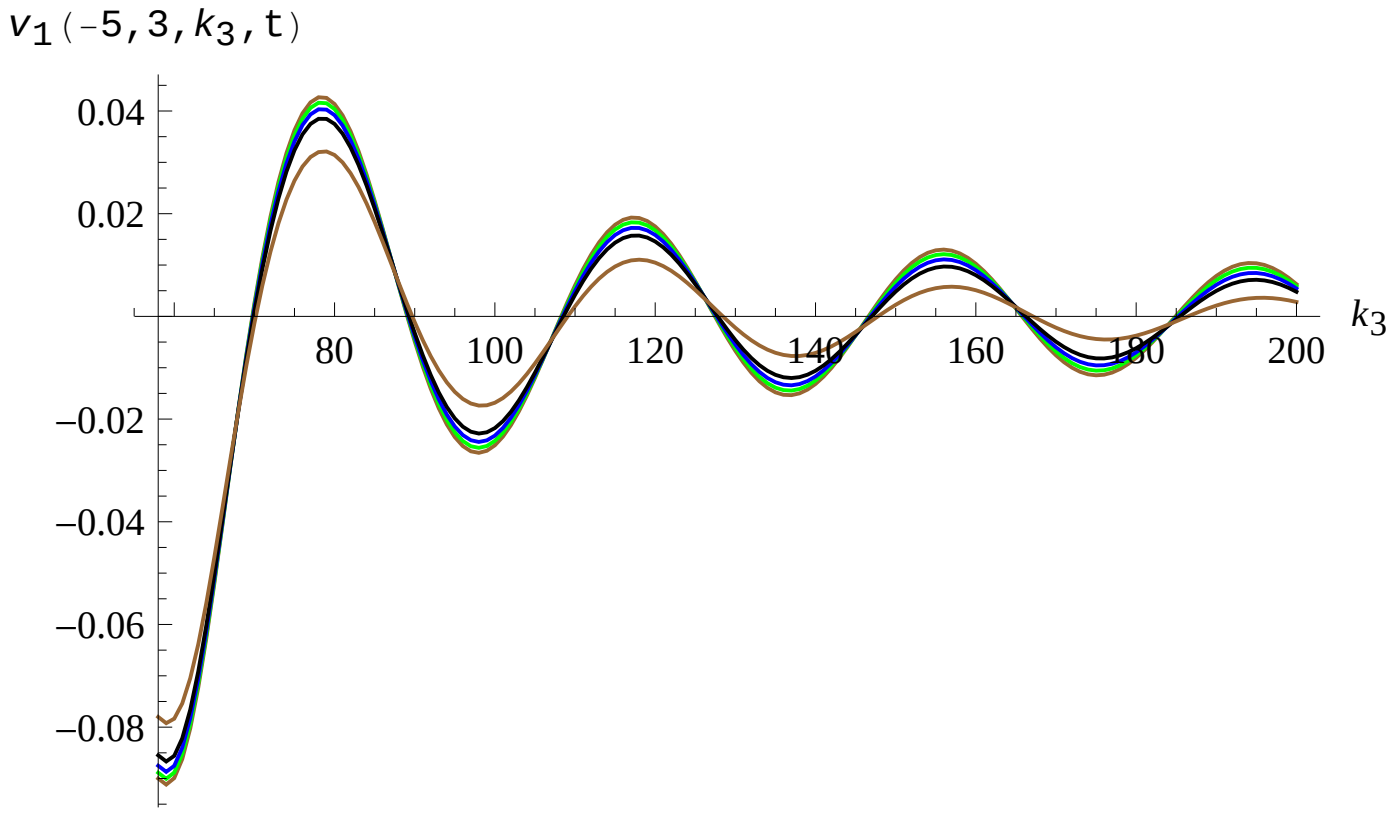

Figure 4: *Type II*, $a = 20$, $E_0 = 5 \times 10^4$. $\mathbf{v}_1(\mathbf{k}, t)$ *vs* k_3 *for* k_1, k_2 *fixed, at the times* $t \times 10^7 = 1342, 1500, 1544, 1574, 1600$. *The amplitudes increase as time grows, and tend to a limit. Simulation range* $k_3 \in [-19, 3028]$.

3. Li-Sinai solutions: simulations. Type I: compared growth.

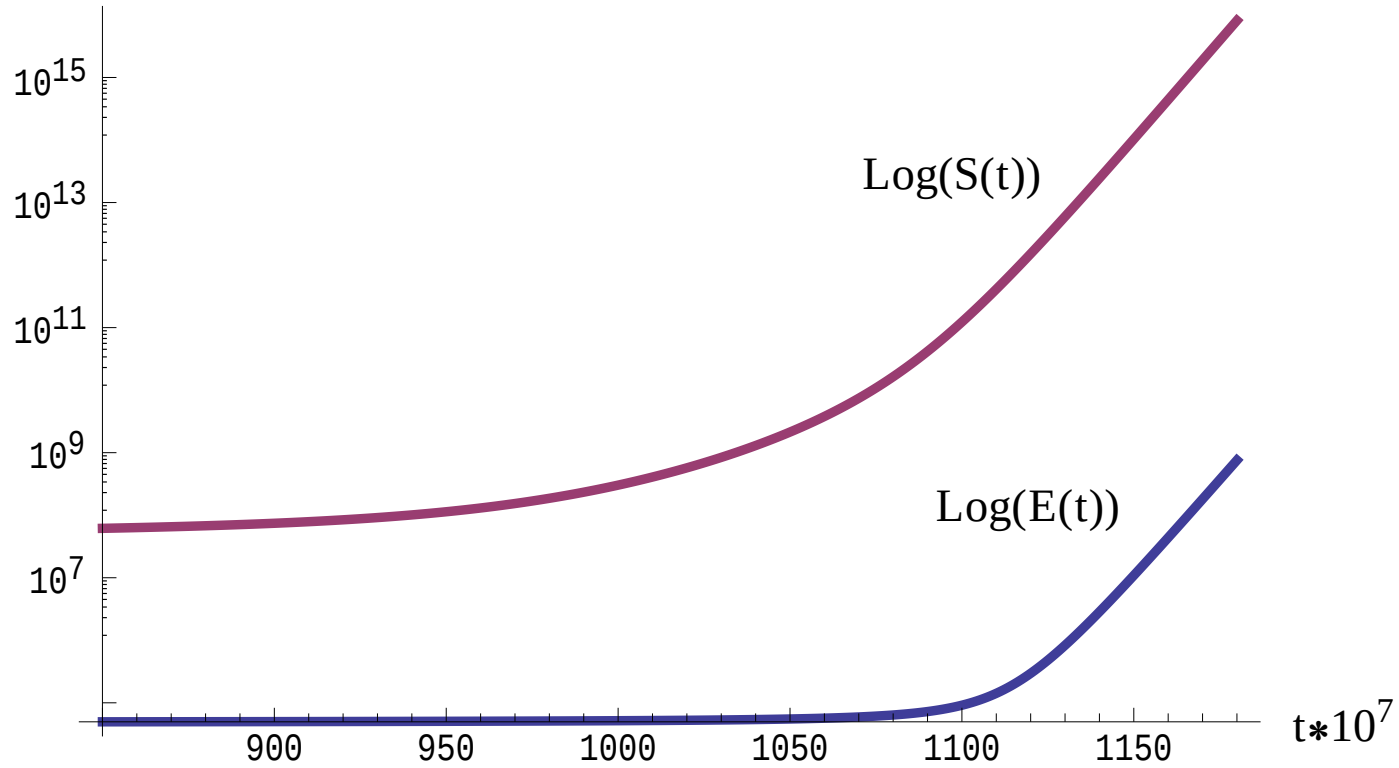

Figure 5: *Type I*, $a = 20$, $E_0 = 5 \times 10^4$. *Compared growth of the total enstrophy* $S(t)$ *and the total energy* $E(t)$. *Simulation range* $k_3 \in [-19, 2528]$.

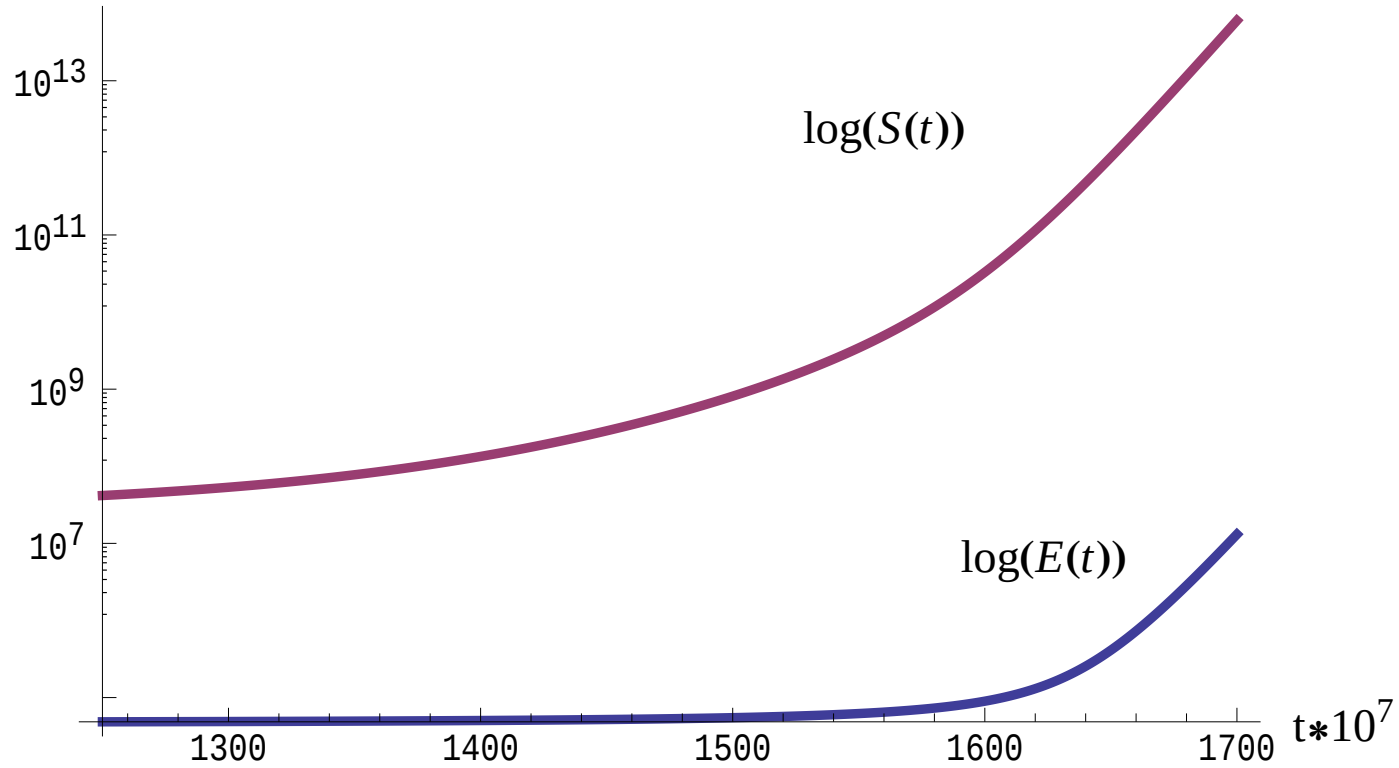

Figure 6: *Type II*, $a = 20$, $E_0 = 5 \times 10^4$. *Compared growth of the total enstrophy* $S(t)$ *and the total energy* $E(t)$. *Simulation range* $k_3 \in [-19, 2528]$.

3. Li-Sinai solutions: simulations. Enstrophy distribution

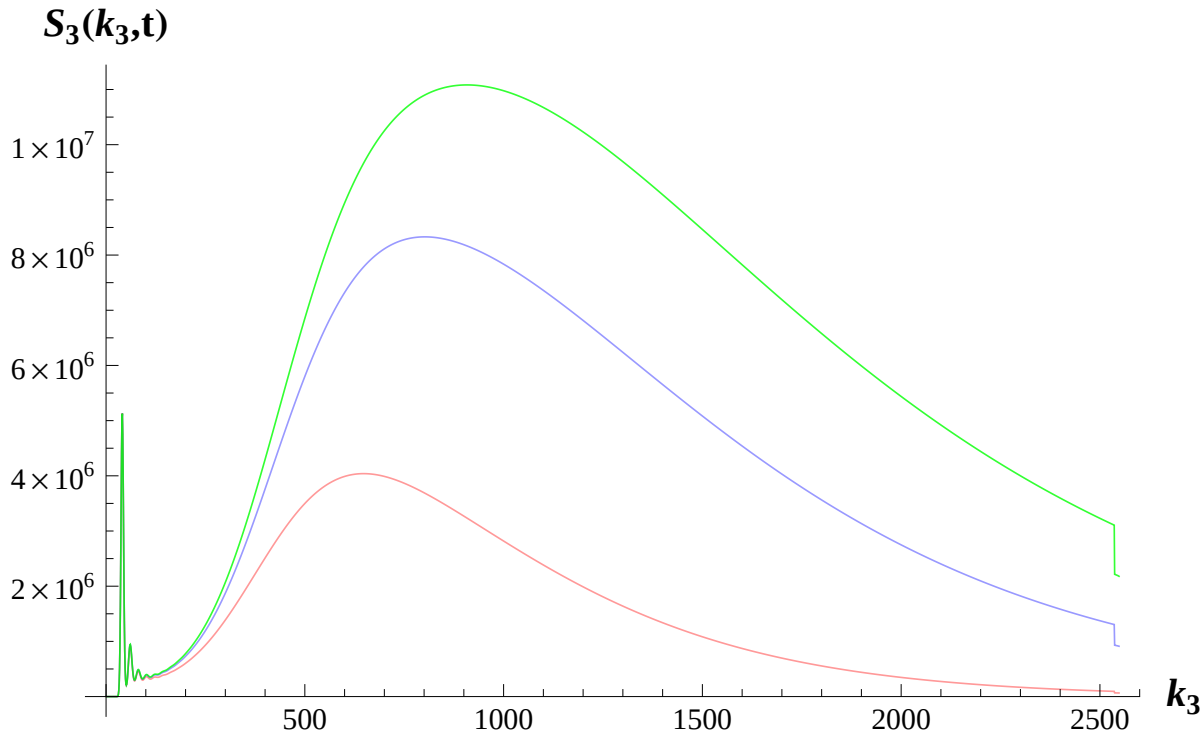

Figure 7: *Type I*, $a = 20$, $E_0 = 5 \times 10^4$. *Plot of the marginal enstrophy density* $S_3(k_3, t)$ *on the whole simulation range* $-19 \leq k_3 \leq 2528$, *at* $t \cdot 10^7 = 1060, 1075, 1080$.

3. Li-Sinai solutions: simulations. Enstrophy distribution

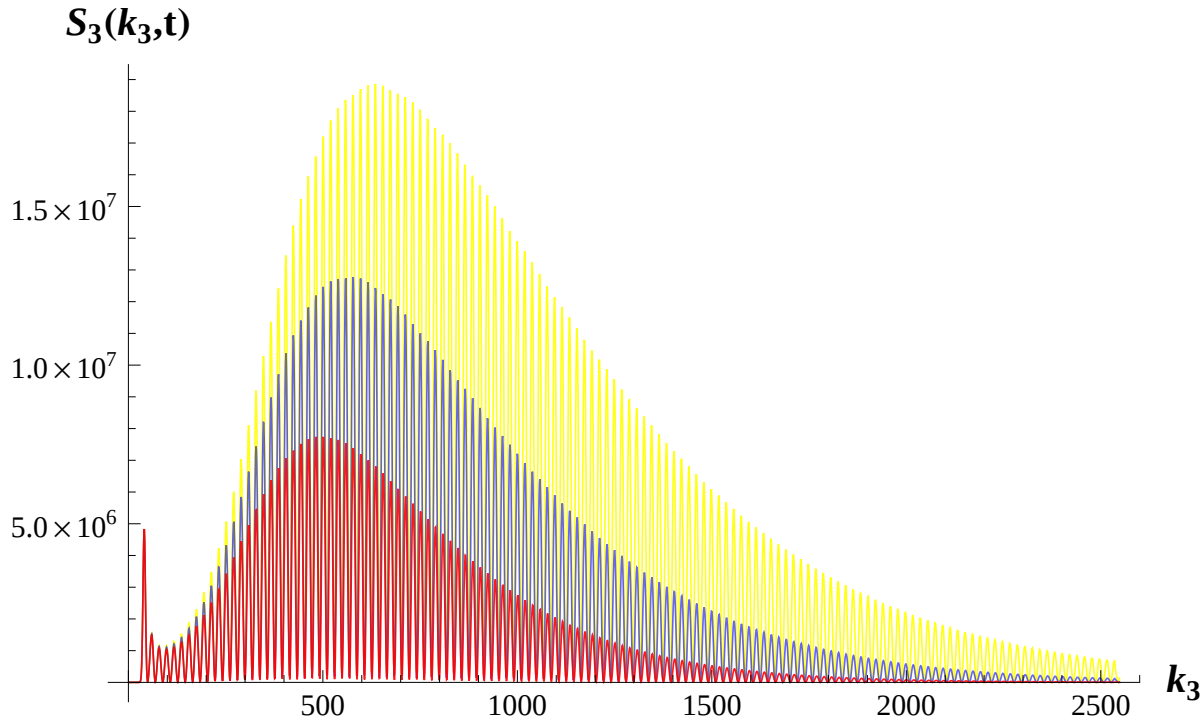

Figure 8: *Type II*, $a = 20$, $E_0 = 5 \times 10^4$. *Plot of the marginal enstrophy density* $S_3(k_3, t)$ *on the whole simulation range* $-19 \leq k_3 \leq 2528$, *at* $t \cdot 10^7 = 1521, 1544, 1560$.

3. Li-Sinai solutions: simulations. Enstrophy distribution.

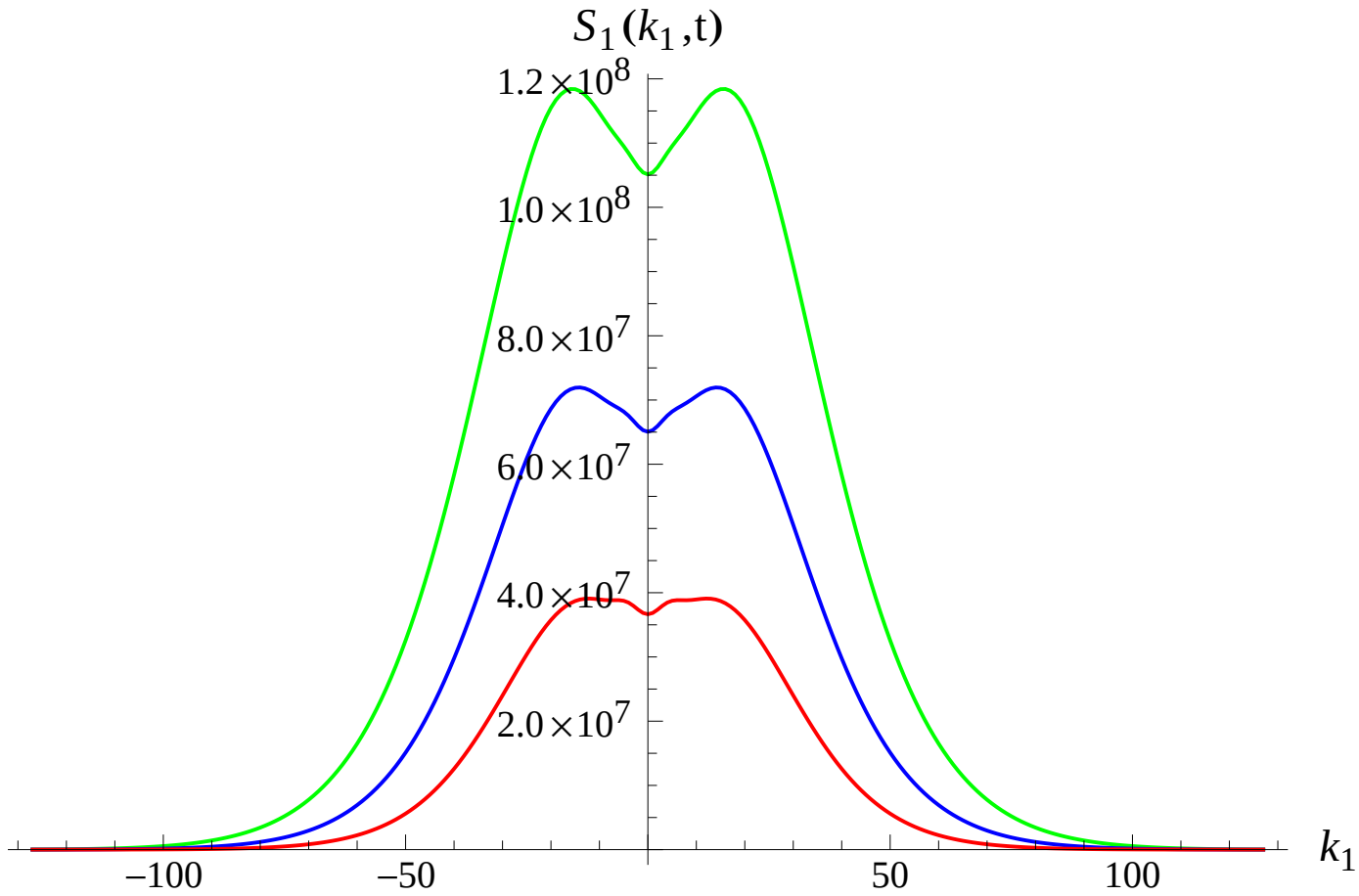

Figure 9: *Type II*, $a = 20$, $E_0 = 5 \times 10^4$. *Plot of the marginal enstrophy density* $S_1(k_1, t)$ *at* $t \cdot 10^7 = 1521, 1544, 1560$. *Simulation range* $k_3 \in [-19, 2528]$.

The divergence of $E(t), S(t)$ is due to the large k_3 modes, and it is hard to follow on the computer.

The divergence of $E(t), S(t)$ is due to the large k_3 modes, and it is hard to follow on the computer.

In fact, while $S(t)$ shows a significant growth before the significant support gets out of the simulation region, the growth of $E(t)$ is hard to follow with the present computer resources.

The divergence of $E(t), S(t)$ is due to the large k_3 modes, and it is hard to follow on the computer.

In fact, while $S(t)$ shows a significant growth before the significant support gets out of the simulation region, the growth of $E(t)$ is hard to follow with the present computer resources.

The best way of estimating the critical time τ is based on the fact that, as predicted by the theory, the high k_3-modes fall off exponentially fast in k_3 with a rate proportional to $(\tau - t)$.

The divergence of $E(t), S(t)$ is due to the large k_3 modes, and it is hard to follow on the computer.

In fact, while $S(t)$ shows a significant growth before the significant support gets out of the simulation region, the growth of $E(t)$ is hard to follow with the present computer resources.

The best way of estimating the critical time τ is based on the fact that, as predicted by the theory, the high k_3-modes fall off exponentially fast in k_3 with a rate proportional to $(\tau - t)$.

Already at times relatively far from the critical time, the decay rate of the marginal energy density $E_3(k_3, t)$ in the region $k_3 > 400$ turns out to be exponential decreasing in time with great accuracy.

The divergence of $E(t), S(t)$ is due to the large k_3 modes, and it is hard to follow on the computer.

In fact, while $S(t)$ shows a significant growth before the significant support gets out of the simulation region, the growth of $E(t)$ is hard to follow with the present computer resources.

The best way of estimating the critical time τ is based on the fact that, as predicted by the theory, the high k_3-modes fall off exponentially fast in k_3 with a rate proportional to $(\tau - t)$.

Already at times relatively far from the critical time, the decay rate of the marginal energy density $E_3(k_3, t)$ in the region $k_3 > 400$ turns out to be exponential decreasing in time with great accuracy.

The results are remarkably stable with respect to the longitudinal simulation range.

The divergence of $E(t), S(t)$ is due to the large k_3 modes, and it is hard to follow on the computer.

In fact, while $S(t)$ shows a significant growth before the significant support gets out of the simulation region, the growth of $E(t)$ is hard to follow with the present computer resources.

The best way of estimating the critical time τ is based on the fact that, as predicted by the theory, the high k_3-modes fall off exponentially fast in k_3 with a rate proportional to $(\tau - t)$.

Already at times relatively far from the critical time, the decay rate of the marginal energy density $E_3(k_3, t)$ in the region $k_3 > 400$ turns out to be exponential decreasing in time with great accuracy.

The results are remarkably stable with respect to the longitudinal simulation range.

3. Li-Sinai solutions: simulations. Decay rate.

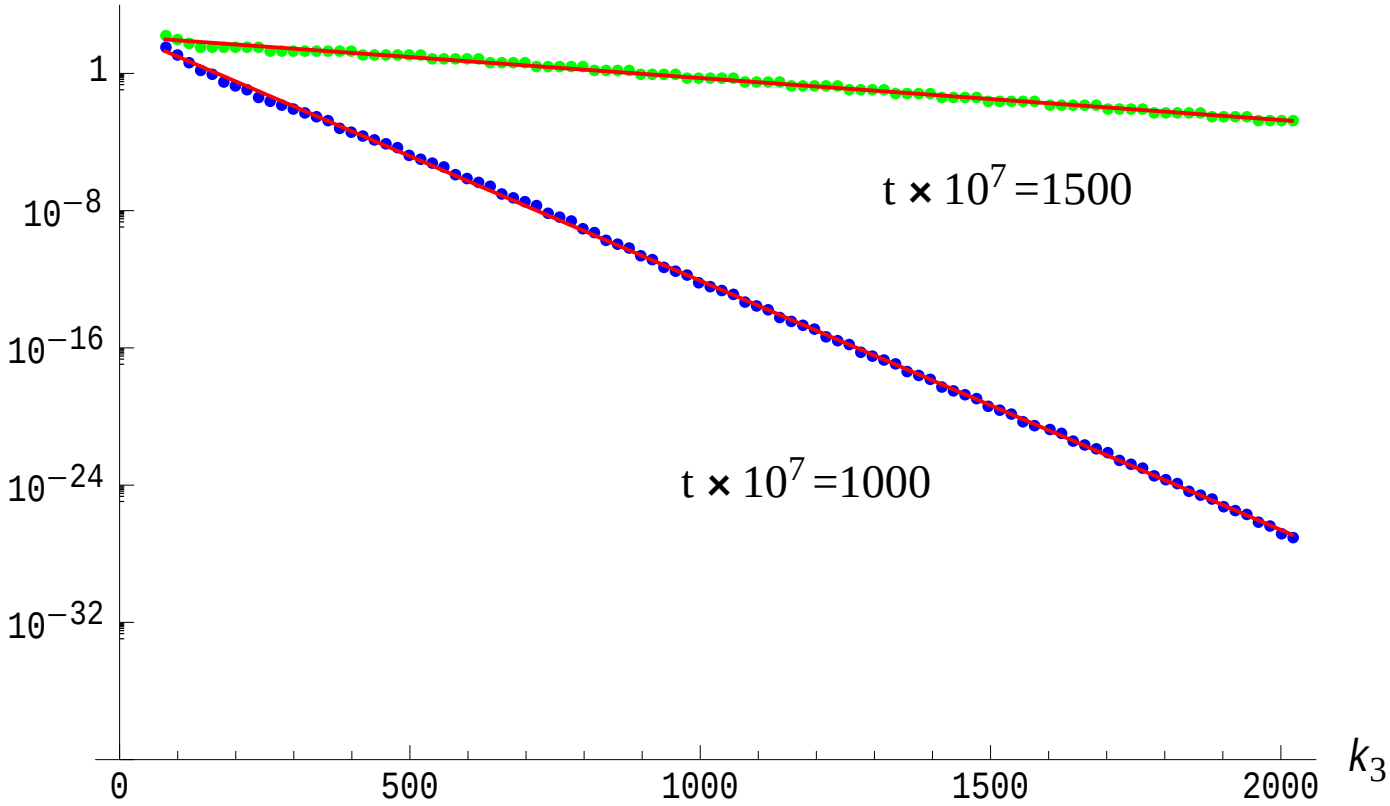

Figure 10: *Type II*, $a = 20$, $E_0 = 5 \times 10^4$. *Plot of* $\log(E_3(k_3, t))$, *where* E_3 *is the marginal energy density along the* k_3*-axis for* $k_3 \geq 400$ *at two different times. The dots represent the local maxima of the oscillations of* $E_3(k_3, t)$. *Simulation range* $k_3 \in [-19, 2028]$.

3. Li-Sinai solutions: simulations. Critical time.

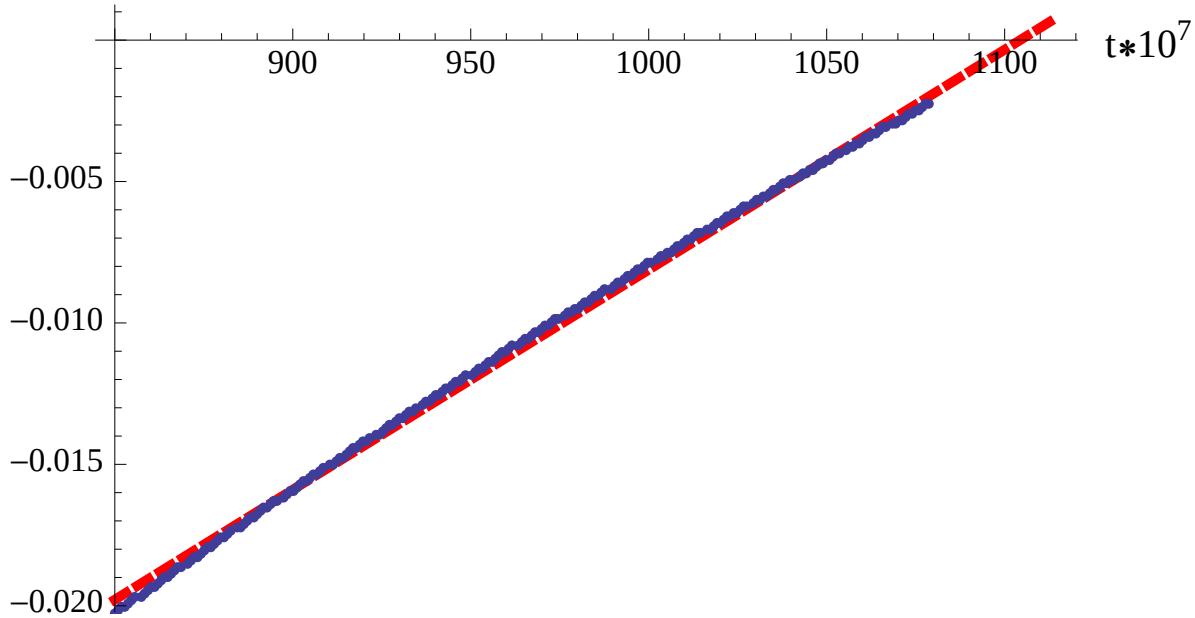

Figure 11: *Type I*, $a = 20$, $E_0 = 5 \times 10^4$. *Exponential decay rate for the marginal density* $E_3(k_3, t)$, *taken for* $k_3 \geq 400$, *vs magnified time* $t \times 10^7$, *with linear regression (dashed line). Simulation range* $k_3 \in [-19, 2528]$.

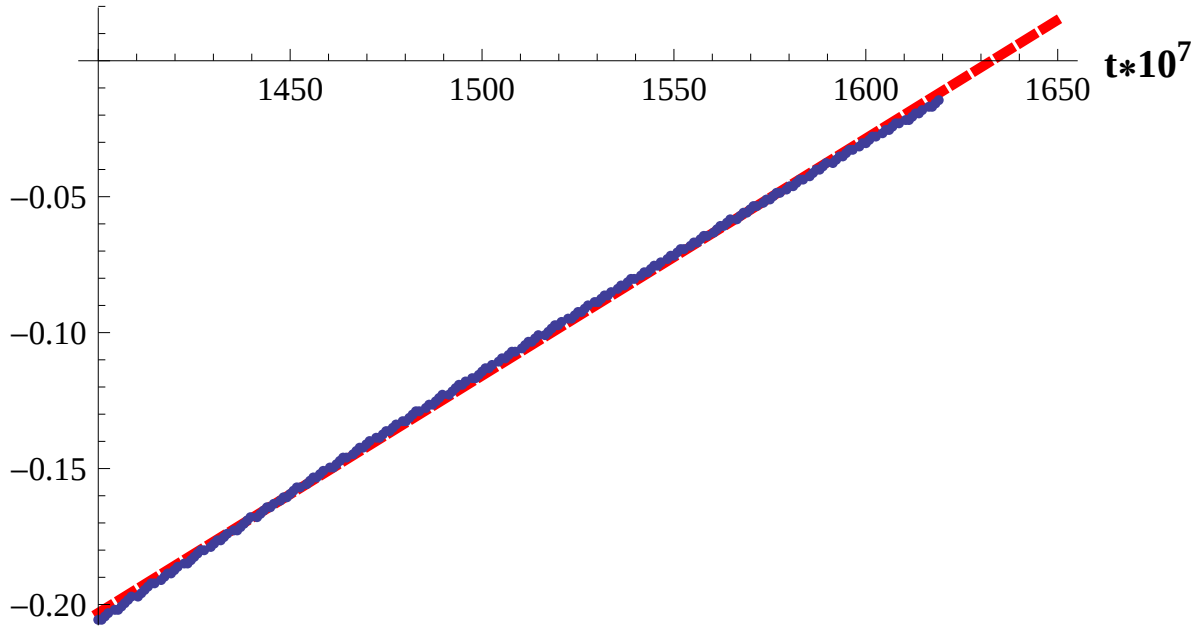

Figure 12: *Type II*, $a = 20$, $E_0 = 5 \times 10^4$. *Exponential decay rate for the marginal density* $E_3(k_3, t)$, *taken for* $k_3 \geq 400$, *vs magnified time* $t \times 10^7$, *with linear regression (dashed line). Simulation range* $k_3 \in [-19, 2528]$.

The estimates for the critical time obtained from the previous plots (case $a = 20$ and $E_0 = 5 \times 10^4$) are:

The estimates for the critical time obtained from the previous plots (case $a = 20$ and $E_0 = 5 \times 10^4$) are:

$\tau \approx 1110 \times 10^{-7}$ for type I and $\tau \approx 1630$ for type II.

The estimates for the critical time obtained from the previous plots (case $a = 20$ and $E_0 = 5 \times 10^4$) are:

$\tau \approx 1110 \times 10^{-7}$ for type I and $\tau \approx 1630$ for type II.

Quite recently we obtained more computer time in the framework of the european project PRACE,

The estimates for the critical time obtained from the previous plots (case $a = 20$ and $E_0 = 5 \times 10^4$) are:

$\tau \approx 1110 \times 10^{-7}$ for type I and $\tau \approx 1630$ for type II.

Quite recently we obtained more computer time in the framework of the european project PRACE, which allows us to study the dependence of the critical time on the parameter a and on the initial energy E_0.

The estimates for the critical time obtained from the previous plots (case $a = 20$ and $E_0 = 5 \times 10^4$) are:

$\tau \approx 1110 \times 10^{-7}$ for type I and $\tau \approx 1630$ for type II.

Quite recently we obtained more computer time in the framework of the european project PRACE, which allows us to study the dependence of the critical time on the parameter a and on the initial energy E_0.

Observe that the parameter a controls the initial enstrophy $S(0)$ independently of the initial energy E_0.

The estimates for the critical time obtained from the previous plots (case $a = 20$ and $E_0 = 5 \times 10^4$) are:

$\tau \approx 1110 \times 10^{-7}$ for type I and $\tau \approx 1630$ for type II.

Quite recently we obtained more computer time in the framework of the european project PRACE, which allows us to study the dependence of the critical time on the parameter a and on the initial energy E_0.

Observe that the parameter a controls the initial enstrophy $S(0)$ independently of the initial energy E_0.

The data show that when we increase a the excitation of the high k_3-modes is accelerated and the critical time decreases

The estimates for the critical time obtained from the previous plots (case $a = 20$ and $E_0 = 5 \times 10^4$) are:

$\tau \approx 1110 \times 10^{-7}$ for type I and $\tau \approx 1630$ for type II.

Quite recently we obtained more computer time in the framework of the european project PRACE, which allows us to study the dependence of the critical time on the parameter a and on the initial energy E_0.

Observe that the parameter a controls the initial enstrophy $S(0)$ independently of the initial energy E_0.

The data show that when we increase a the excitation of the high k_3-modes is accelerated and the critical time decreases (at least in the range we considered).

3. Li-Sinai solutions: simulations. Critical time.

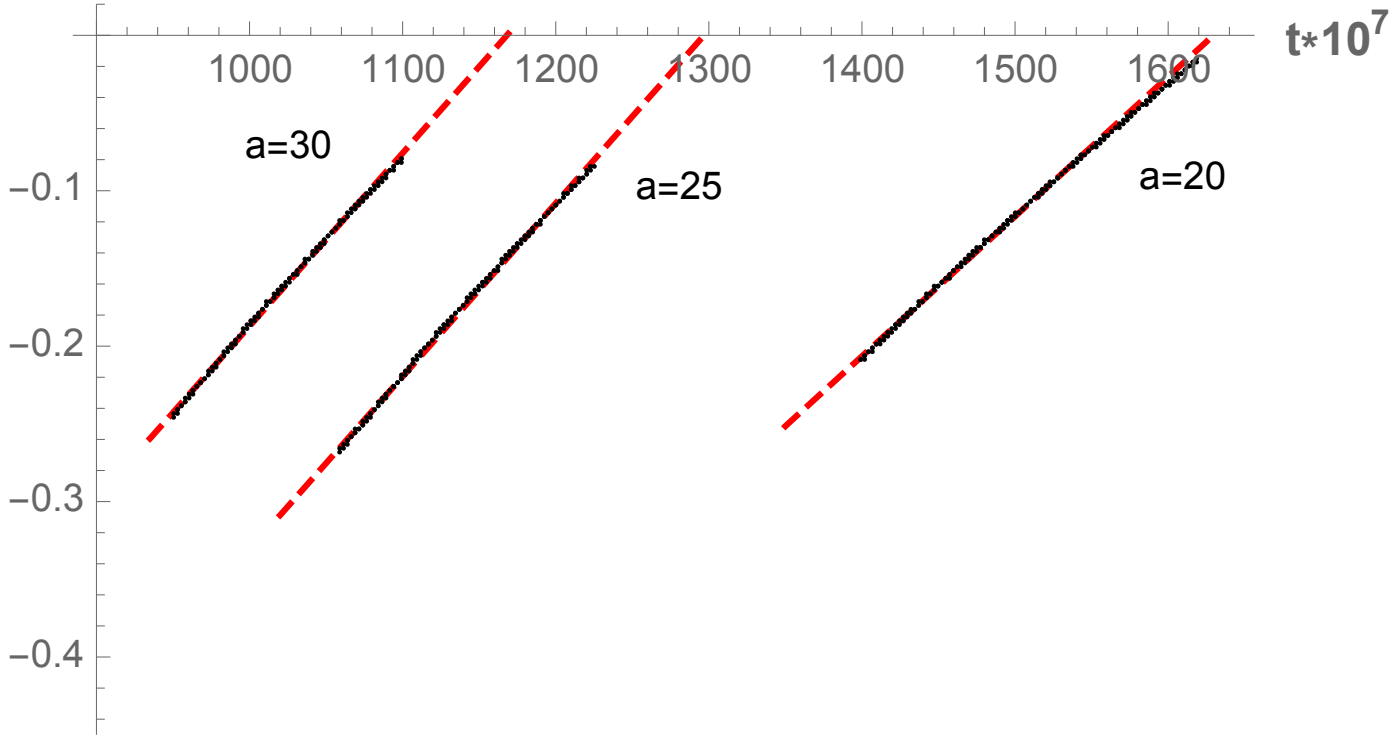

Figure 13: *Type II*, $E_0 = 5 \times 10^4$. *Behavior of the exponential decay rates of* $E_3(k_3, t)$ *vs. magnified time* $t \times 10^7$ *for* $a = 20, 25, 30$. *Simulation range* $k_3 \in [-19, 3028]$

Once we have an estimate τ_* of the critical time, we can check the power-law divergence of $E(t)$ and $S(t)$.

Once we have an estimate τ_* of the critical time, we can check the power-law divergence of $E(t)$ and $S(t)$.

For the growth of $E(t)$ the computer data are insufficient, because the significant growth at the blow-up is mainly due to excitation of the k_3-modes outside the integration range.

Once we have an estimate τ_* of the critical time, we can check the power-law divergence of $E(t)$ and $S(t)$.

For the growth of $E(t)$ the computer data are insufficient, because the significant growth at the blow-up is mainly due to excitation of the k_3-modes outside the integration range.

For $S(t)$ we get results that are compatible with the prediction.

Once we have an estimate τ_* of the critical time, we can check the power-law divergence of $E(t)$ and $S(t)$.

For the growth of $E(t)$ the computer data are insufficient, because the significant growth at the blow-up is mainly due to excitation of the k_3-modes outside the integration range.

For $S(t)$ we get results that are compatible with the prediction.

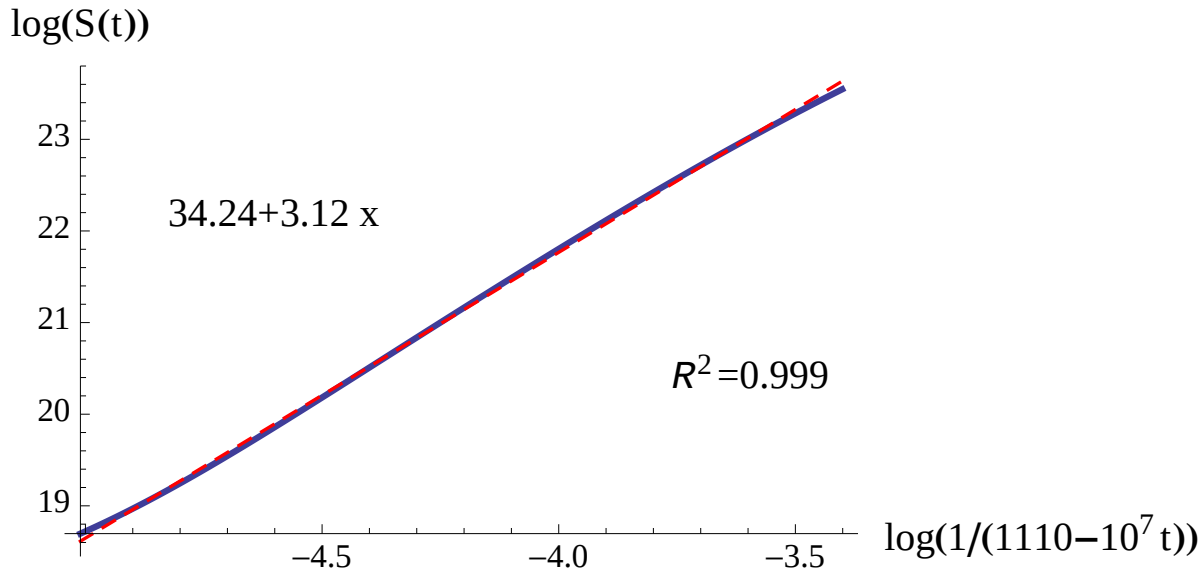

Figure 14: *Type I*, $a = 20$, $E_0 = 5 \times 10^4$. *Log-plot of the total enstrophy* $S(t)$ *vs* $\log \frac{1}{\tau_* - t}$, *at times near the blow-up, with linear regression (dashed line, the prediction for the slope is* 3.0*). Simulation range* $k_3 \in [-19, 2528]$.

For the behavior in **x**-space the data show convergence everywhere as $t \uparrow \tau$, except for a singularity at the origin for type *I* solutions

For the behavior in **x**-space the data show convergence everywhere as $t \uparrow \tau$, except for a singularity at the origin for type *I* solutions and at two points

$$\mathbf{x}_{\pm}^{(0)} = (0, 0, \pm x_3^{(0)}), \qquad x_3^{(0)} \approx \frac{\pi}{a}$$

for the solutions of type II.

3. Li-Sinai solutions: simulations. x-space.

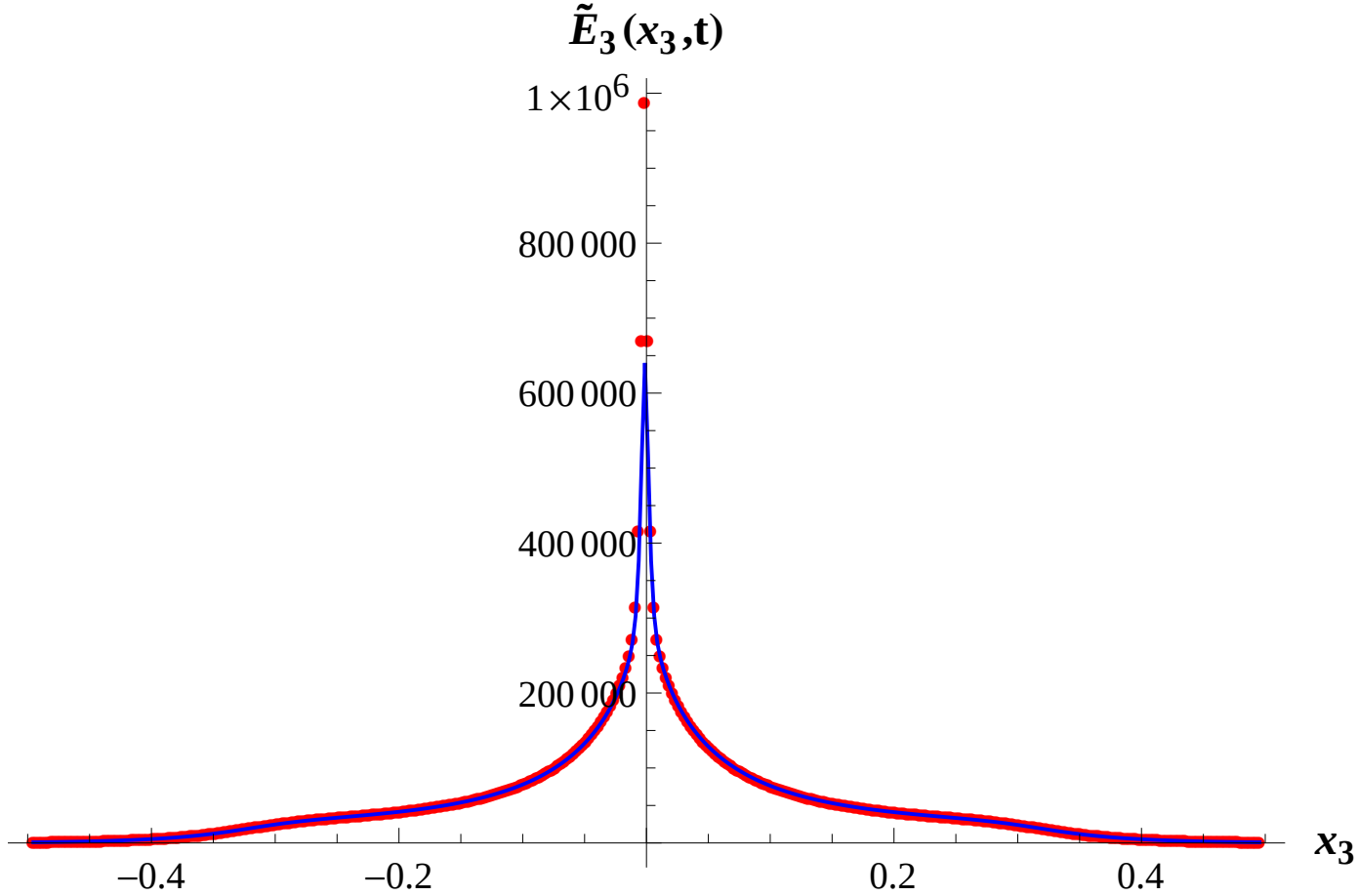

Figure 15: *Type I*, $a = 20$, $E_0 = 5 \times 10^4$. *Plot of the marginal energy density* $\tilde{E}_3(x_3, t)$ *at* $t \cdot 10^7 = 1021$ *(dotted line) and* $t \times 10^7 = 1044$ *(continuous line). Simulation range* $k_3 \in [-19, 2528]$.

3. Li-Sinai solutions: simulations. x-space.

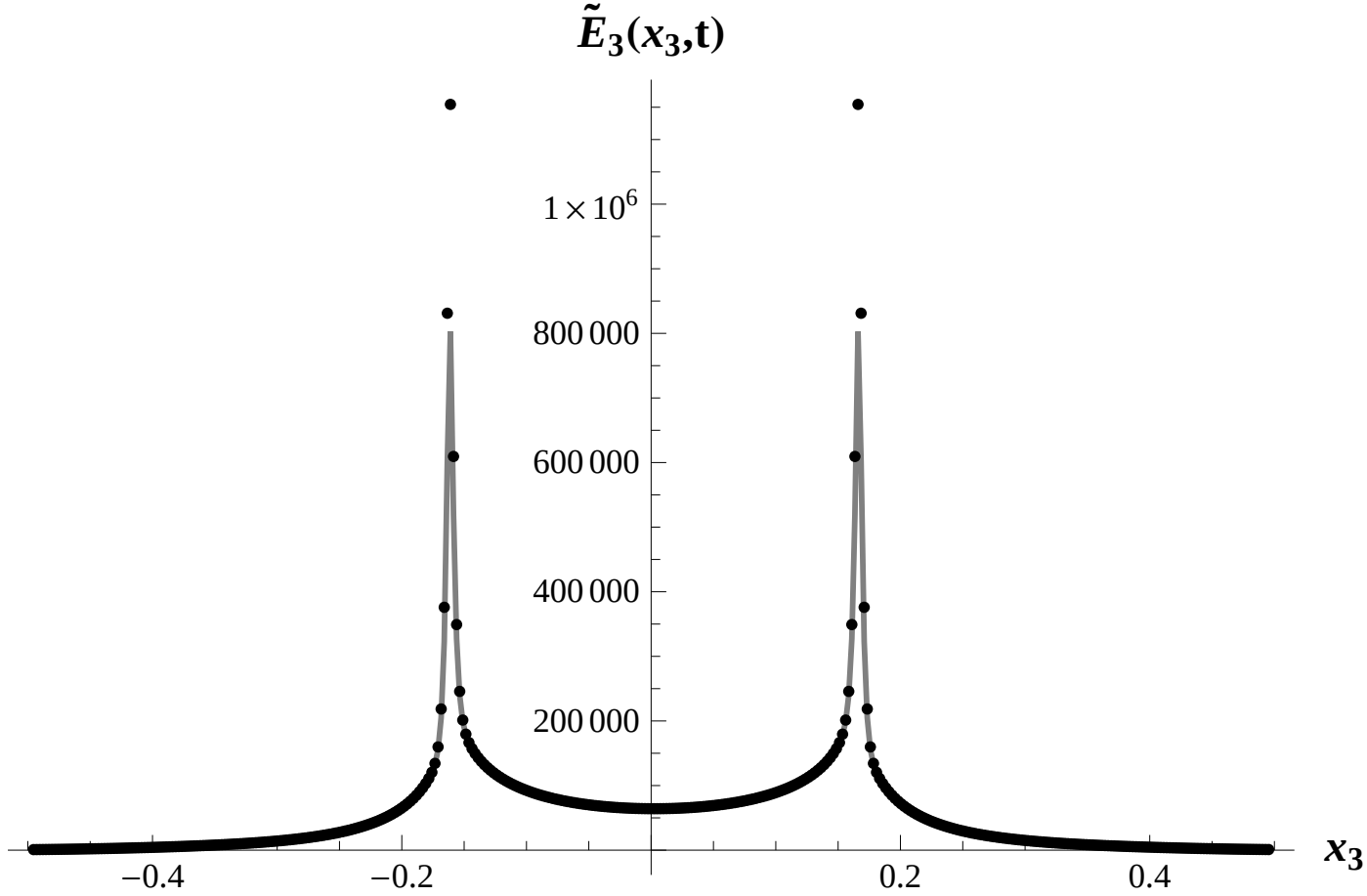

Figure 16: *Type II*, $a = 20$, $E_0 = 5 \times 10^4$. *Plot of the marginal energy density* $\tilde{E}_3(x_3, t)$ *at* $t \cdot 10^7 = 1521$ *(continuous line) and* $t \times 10^7 = 1544$ *(dotted line). Simulation range* $k_3 \in [-19, 2528]$

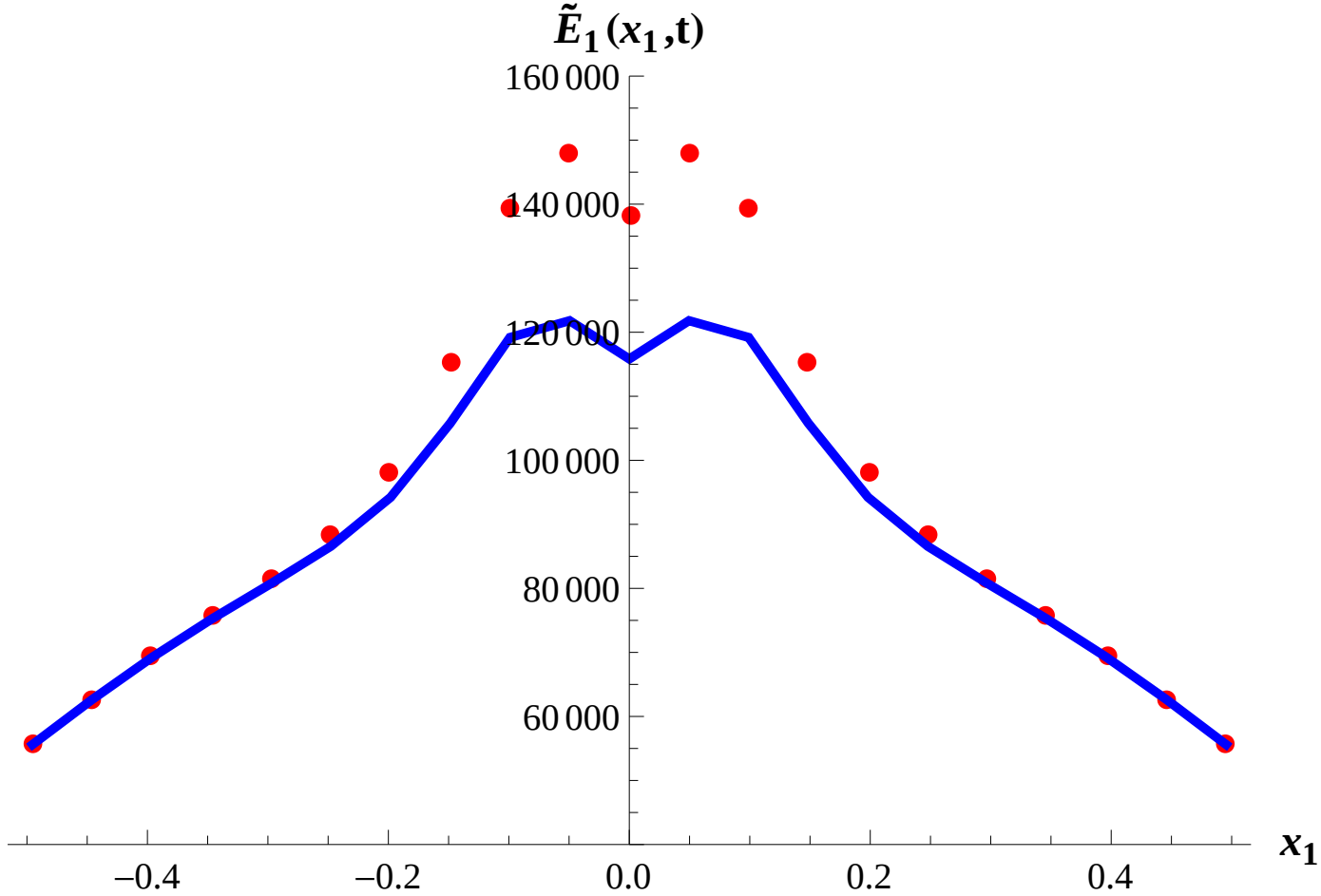

Figure 17: *Type II*, $a = 20$, $E_0 = 5 \times 10^4$. *Plot of the marginal energy density* $\tilde{E}_1(x_1, t)$ *at* $t \cdot 10^7 = 1521$ *(continuous line), and* $t \cdot 10^7 = 1544$ *(dotted line). Simulation range* $k_3 \in [-19, 2528]$.

4. REAL SOLUTIONS.

Assuming antisymmetric initial data $A\mathbf{v}_0(\mathbf{k})$

$$\mathbf{v}_0(\mathbf{k}) = \mathbf{v}_0^{\pm}(\mathbf{k}) - \mathbf{v}_0^{\pm}(-\mathbf{k}),$$

4. REAL SOLUTIONS.

Assuming antisymmetric initial data $A\mathbf{v}_0(\mathbf{k})$

$$\mathbf{v}_0(\mathbf{k}) = \mathbf{v}_0^{\pm}(\mathbf{k}) - \mathbf{v}_0^{\pm}(-\mathbf{k}),$$

where $\mathbf{v}_0^{\pm}$ are as above, we get a real solution.

4. REAL SOLUTIONS.

Assuming antisymmetric initial data $A\mathbf{v}_0(\mathbf{k})$

$$\mathbf{v}_0(\mathbf{k}) = \mathbf{v}_0^{\pm}(\mathbf{k}) - \mathbf{v}_0^{\pm}(-\mathbf{k}),$$

where $\mathbf{v}_0^{\pm}$ are as above, we get a real solution. (The choice $\pm$ amounts to a change of sign.)

4. REAL SOLUTIONS.

Assuming antisymmetric initial data $A\mathbf{v}_0(\mathbf{k})$

$$\mathbf{v}_0(\mathbf{k}) = \mathbf{v}_0^{\pm}(\mathbf{k}) - \mathbf{v}_0^{\pm}(-\mathbf{k}),$$

where $\mathbf{v}_0^{\pm}$ are as above, we get a real solution. (The choice $\pm$ amounts to a change of sign.) $\mathbf{v}_0(\mathbf{k})$ has support in two separate regions around the points $\pm(0, 0, a)$.

4. Real solutions.

We can predict that some properties of the complex solutions still hold:

4. Real solutions.

We can predict that some properties of the complex solutions still hold:
- The support in **k**-space restricted to a thin (double) cone around the main axis,

4. Real solutions.

We can predict that some properties of the complex solutions still hold:

- The support in $\mathbf{k}$-space restricted to a thin (double) cone around the main axis,

- The solution shows modulated oscillations along the k_3-axis, as the complex solutions of type *II*.

The simulation show, if the initial energy is large enough, that:

The simulation show, if the initial energy is large enough, that:

- The total enstrophy $S(t)$ grows, reaches a maximum at a time t_* (which for a fixed depends on E_0), then falls;

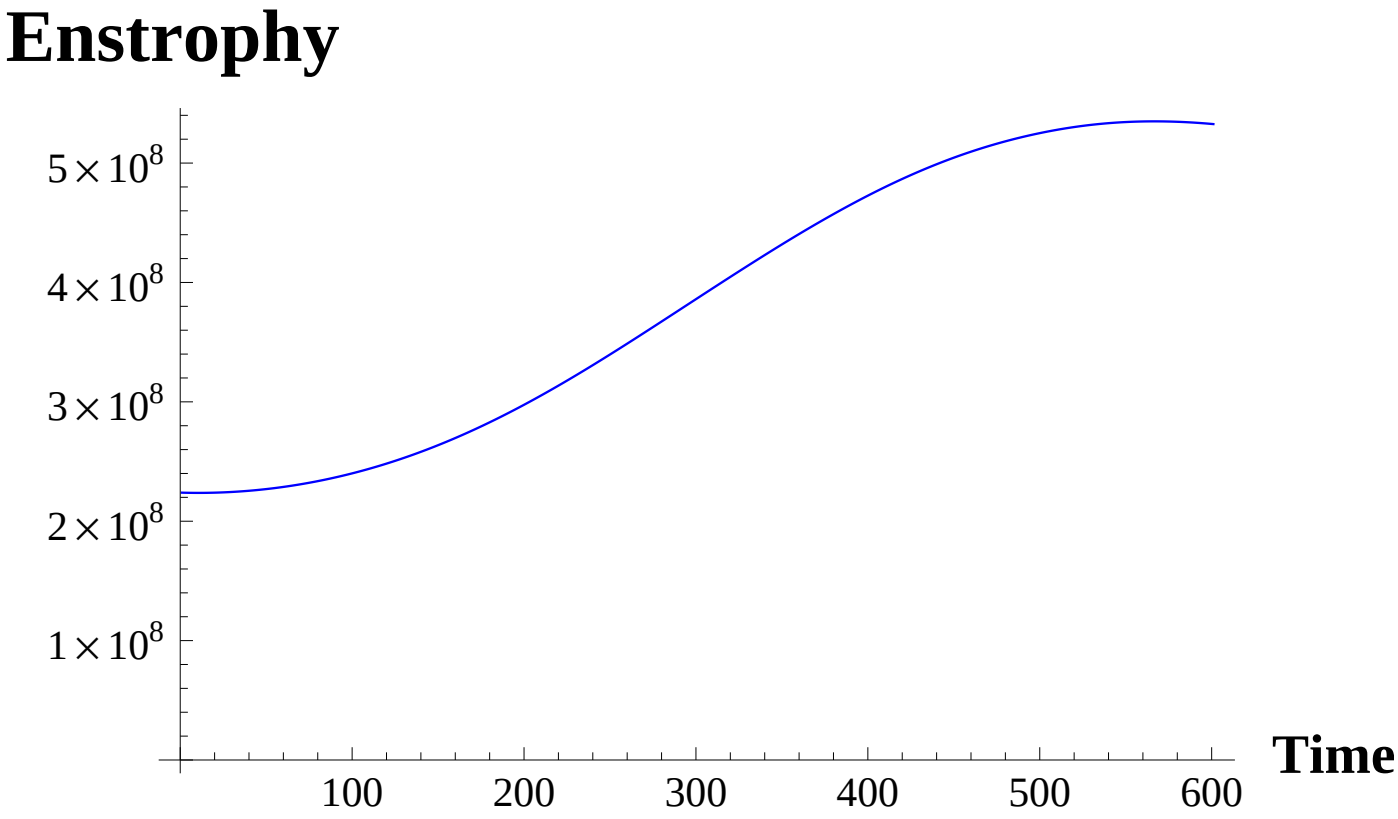

Figure 18: *Plot of the total enstrophy $S(t)$ vs. magnified time $t \times 3.2 \times 10^7$. Initial energy $\bar{E}_0 = 2.5 \times 10^4$, $a = 20$.*

- The large k_3 modes fall off exponentially fast, with a rate decreasing in absolute value up to $t \approx t_*$, then stays constant.

4. Real solutions.

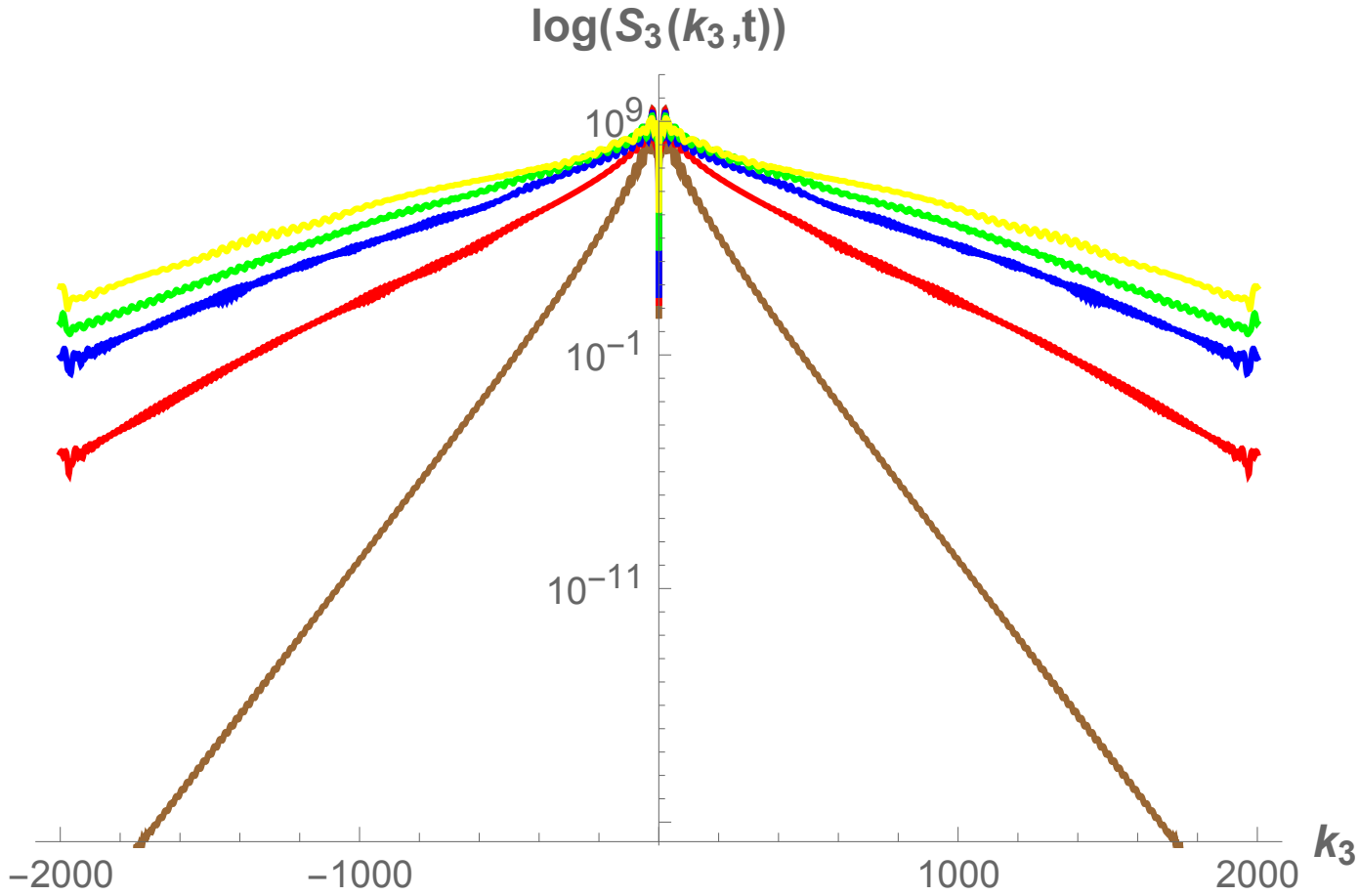

Figure 19: *Logarithmic plot of the marginal density* $\tilde{E}_3(k_3, t)$ *at the (magnified) times* $t \times 3.2 \times 10^7 = 100, 200, 300, 400, 500$. *Initial energy* $\bar{E}_0 = 2.5 \times 10^4$, $a = 20$.

- At the time t_*, the energy and the enstrophy concentrate in two (pseudo)-spikes, close to the singularities of the complex solution of type *II* with the same a.

4. Real solutions.

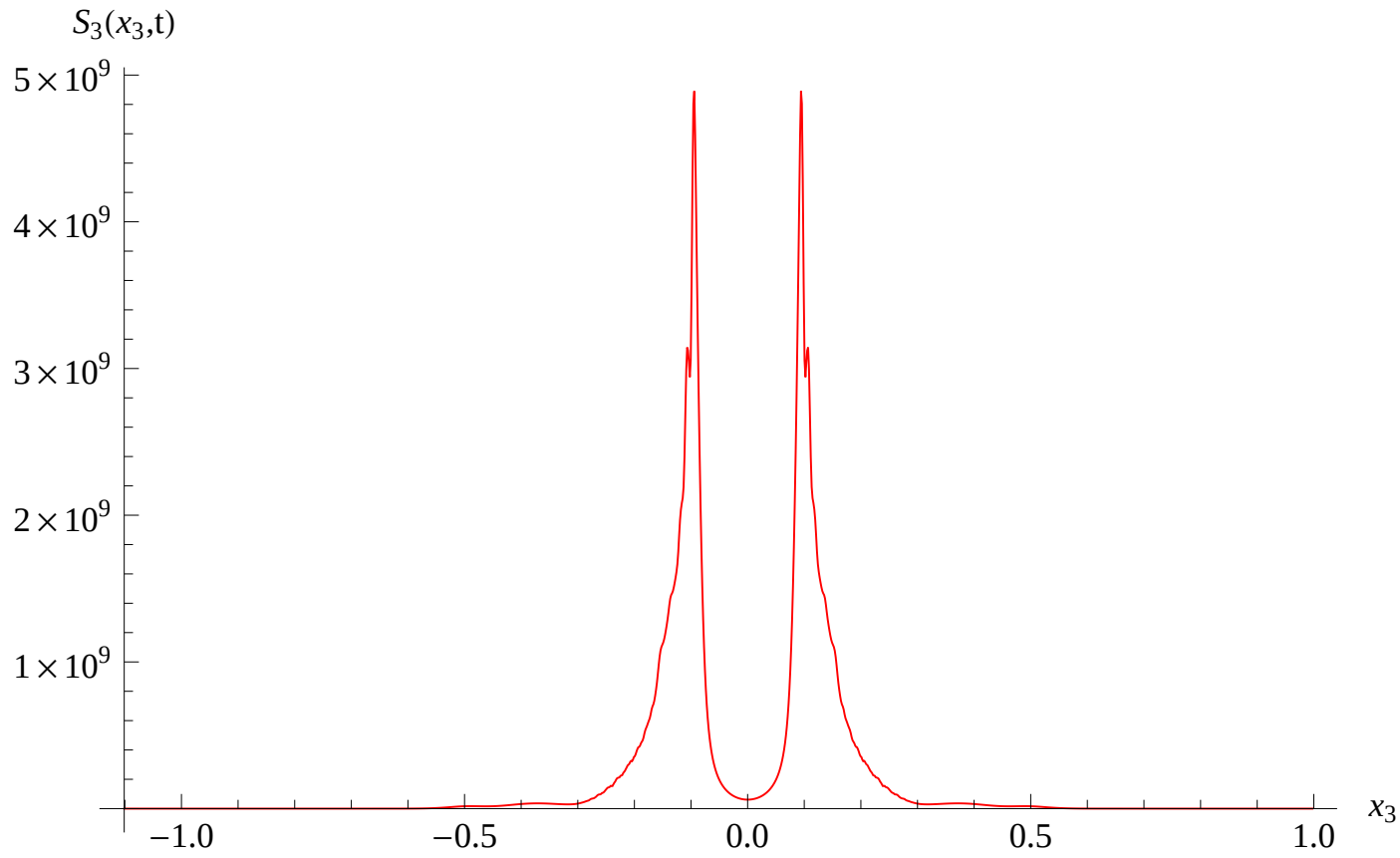

Figure 20: *Plot of the marginal density* $\tilde{S}_3(x_3, t)$ *at* $t = 1.27 \times 10^{-5}$. *Initial energy* $\bar{E}_0 = 2.5 \times 10^4$, $a = 20$.